

# Bohmian analysis of dark solutions in interfering Bose-Einstein condensates: the dynamical role of underlying velocity fields

J. Tounli and A. S. Sanz\*

*Department of Optics, Faculty of Physical Sciences, Universidad Complutense de Madrid  
Pza. Ciencias 1, Ciudad Universitaria – 28040 Madrid, Spain*

(Dated: July 12, 2024)

In the last decades, the experimental research on Bose-Einstein interferometry has received much attention due to promising technological implications. This has thus motivated the development of numerical simulations aimed at solving the time-dependent Gross-Pitaevskii equation and its reduced one-dimensional version to better understand the development of interference-type features and the subsequent soliton dynamics. In this work, Bohmian mechanics is considered as an additional tool to further explore and analyze the formation and evolution in real time of the soliton arrays that follow the merging of two condensates. An alternative explanation is thus provided in terms of an underlying dynamical velocity field, directly linked to the local phase variations undergone by the condensate along its evolution. Although the reduced one-dimensional model is considered here, it still captures the essence of the phenomenon, rendering a neat picture of the full evolution without diminishing the generality of the description. To better appreciate the subtleties of free versus bound dynamics, two cases are discussed. First, the soliton dynamics exhibited by a coherent superposition of two freely released condensates is studied, discussing the peculiarities of the underlying velocity field and the corresponding flux trajectories in terms of both the peak-to-peak distance between the two initial clouds and the addition of a phase difference between them. In the latter case, an interesting correspondence with the well-known Aharonov-Bohm effect is found. Then, the recurrence dynamics displayed by the more general case of two condensates released from the two opposite turning points of a harmonic trap is considered in terms of the distance between such turning points. In both cases, it is presumed that the initial superposition state is generated by splitting adiabatically a single condensate with the aid of an optical lattice, which is then turned off. Nonetheless, although the lattice does not play any active role in the simulations, the parameters defining the initial states are in compliance with it, which helps in the interpretation and understanding of the results observed.

## I. INTRODUCTION

In the late 1990s, Ketterle and coworkers [1, 2] produced the first experimental realization of interference with a Bose-Einstein condensate (BEC). As they showed, when an ultracold atomic cloud is coherently split up and then the two resulting separate clouds are released again, the latter interact in such a way that a pattern of alternating bands of more and less atomic density can be observed. To some extent, an analogy can be established between this behavior and the interference fringes observed in a typical Young-type two-slit experiment, although the latter case obeys a linear dynamics, while the former is a consequence of a nonlinear one. A similar effect can also be observed by splitting the condensate and then letting one of the parties to drop on top of the other, as it was shown by Javanainen *et al.* [3, 4] by the same time. Since the performance of these crucial experiments, interferometry with BECs [5–8] has become an important test ground for the understanding of quantum coherence as well as a remarkable source of novel quantum technology, because of its extraordinary sensitivity, with applications in atom lasers [9] or quantum metrology [10], where the manipulation and preparation of BECs in optical lattices plays a major role [11, 12].

In order to understand and describe the dynamics exhibited by BECs in real time, the Gross-Pitaevskii equation (GPE) constitutes an ideal and simple working tool, without requiring a further many-body description of the full atomic cloud (involving of the order of  $10^3$  to  $10^6$  atoms, in general terms). This is possible by recasting the many-body problem in the form of an effective nonlinear Schrödinger equation, which accounts for the dynamics displayed by a single atom from the cloud acted by an external potential plus a self-interaction term that represents the collective action of any other identical atom from the cloud [5–7]. Because the GPE is not analytical in general, a number of numerical techniques have been considered in the literature to solve this equation and extract useful information from it [13–15]. To some extent, these techniques are analogous to those earlier on applied to solve the time-dependent Schrödinger equation, and have been used recently to study, analyze and describe different aspects involved in BEC interferometry [16–19], the BEC dynamics in periodic and harmonic potentials [20], or the role of the nonlinearity when weakly harmonic and Gaussian traps are considered [21, 22].

Within this context, a suitable tool to understand the dynamics displayed in real time by BECs is the Bohmian formulation of quantum mechanics [23, 24]. The hydrodynamic language introduced by this quantum formulation allows us to understand the interference dynamics leading to the appearance of solitons in terms of an

---

\* Corresponding author: a.s.sanz@fis.ucm.es

underlying velocity field, associated with the phase of the condensate, and to follow its subsequent evolution in time by means of swarms of trajectories. It was shown by Benseny *et al.* [25] that these trajectories constitute a convenient tool to determine how each element of the condensate (not to be confused with each individual atom itself) moves apart, thus providing some clues on its dynamical evolution beyond more conventional-type information, such as the density distribution. In other words, it is possible to determine which portions in the BEC are going to separate faster or slower at each time by simply observing local variations in the underlying velocity field.

In this work we investigate by means of a series of numerical simulations the formation of dark solitons both from two freely released condensates and also under the action of an underlying harmonic trap in order to study the appearance and persistence of recurrences in time. The appearance of soliton-type solutions is associated with the value of the scattering length,  $a_s$ . Specifically, if  $a_s < 0$ , as it happens in  $^{85}\text{Rb}$  [26] or  $^7\text{Li}$  [27], atomic interactions are attractive and bright soliton solutions (spike-type deformations in the density) can appear. On the contrary, for  $a_s > 0$ , as it is the case of  $^{87}\text{Rb}$  [28] or  $^{23}\text{Na}$  [29], the interactions are repulsive, which corresponds to a situation where dark solitons (dips in the density) can be observed. The first experimental observation of dark solitons dates back to 25 years ago, where these solitons were produced in an elongated (cigar shaped) BEC by the so-called phase imprinting method [30]. A year before, though, Scott *et al.* [31] identified the formation of persistent dark fringes in the case of the collision of two separated condensates under the influence of a harmonic trap. This work showed evidence of the relationship between the dark solitons and the phase change, an idea that is implicit in the phase imprinting method devised to generate vortices in the condensate [32], but that also led to the experimental generation of dark solitons [30]. An overview of the advances in dark soliton dynamics both experimentally and theoretically can be found in [33, 34]. Such phase imprinting methods are actually strongly connected to the Bohmian trajectories here. As it is shown below, these trajectories will allow us to monitor in real time some features that are not evident at a first glance from the usual density distributions, and also to elucidate some important differences between the nonlinear and linear dynamical regimes that characterize the BEC dynamics in harmonic traps. This is by virtue of the relationship between the trajectories and the local phase of the condensate. Indeed, pioneering work by Tsuzuki [35] in the early 1970s on the derivation of soliton-like solutions of the Gross-Pitaevskii equation are strongly connected to this formulation (Tsuzuki's is only a first approximation to the exact approach here considered).

The work has been organized as follows. In Sec. II the model and computational details are introduced as well as some elementary notions of the Bohmian formulation. In Sec. III the results obtained from the numerical simu-

lations carried out for the two scenarios mentioned above, namely, free propagation and motion inside a harmonic trap, are presented and discussed. To conclude, some final remarks are summarized in Sec. IV.

## II. THEORY

### A. The reduced one-dimensional GPE

Within the Hartree-Fock approximation, the dynamics of a BEC consisting of  $N$  identical atoms with mass  $m$  is described by the Gross-Pitaevskii equation [5],

$$i\hbar \frac{\partial \Psi(\mathbf{r}, t)}{\partial t} = \left[ -\frac{\hbar^2}{2m} \nabla^2 + V_{\text{ext}}(\mathbf{r}, t) + g\mathcal{N}(\mathbf{r}, t) \right] \Psi(\mathbf{r}, t), \quad (1)$$

where  $V_{\text{ext}}$  describes any external interaction acting on the BEC (e.g., the confining optical trap), while the nonlinear term  $g\mathcal{N}(\mathbf{r}, t)$  accounts for the self-interaction contribution, i.e., the effective interaction with the remaining  $N - 1$  atoms in the cloud. The strength of such interaction is determined by the coupling constant  $g = 4\pi\hbar^2 a_s/m$ , with  $a_s$  being the scattering length [7]. For convenience, the wave function (order parameter) can be recast in polar form, as

$$\Psi(\mathbf{r}, t) = \sqrt{\mathcal{N}(\mathbf{r}, t)} e^{i\theta(\mathbf{r}, t)}, \quad (2)$$

which enables a description of the condensate in terms of its density distribution,  $\mathcal{N}(\mathbf{r}, t) = |\Psi(\mathbf{r}, t)|^2$ , with  $\int |\Psi(\mathbf{r}, t)|^2 d\mathbf{r} = N$ , and its local phase variations, accounted for by  $\theta(\mathbf{r}, t)$ . Here, for numerical convenience, we have chosen the wave function to be normalized to unity, which implies that the factor  $N$  arising from  $\mathcal{N}(\mathbf{r}, t)$  will be included as a multiplicative constant in  $g$ , that is, from now on  $g = 4\pi\hbar^2 a_s N/m$ .

Consider that a prolate configuration for the condensate, which arises assuming typical frequency ranges  $f_z \sim 20 - 60$  Hz and  $f_{\perp} \sim 400 - 900$  Hz. Accordingly, the transverse harmonic trap values will be much larger than the longitudinal one, since  $\omega_{\perp}^2 \gg \omega_z^2$ , and hence, for the times considered, the transverse degrees of freedom can be assumed to be frozen. This thus allows us to provide an effective description of the condensate dynamics along the  $z$ -direction by means of a reduced one-dimensional (1D) GPE [7], which reads as

$$i\hbar \frac{\partial \psi(z, t)}{\partial t} = \left[ -\frac{\hbar^2}{2m} \frac{\partial^2}{\partial z^2} + V_{\text{ext}}(z) + g_{1D}n(z, t) \right] \psi(z, t), \quad (3)$$

where  $g_{1D} = g/2\pi a_{\perp}^2 = 2\hbar\omega_{\perp} a_s$ , with  $a_{\perp} = \sqrt{\hbar/m\omega_{\perp}}$ , is an effective 1D coupling constant that arises from the dimensional reduction of Eq. (1) [36, 37] (see further details about the potential parameters in Sec. II C). From now on, for computational convenience we assume that the wave function  $\psi(z, t)$  is normalized to unity, i.e.,  $\int |\psi(z, t)|^2 dz = \int n(z, t) dz = 1$ , with  $n(z, t)$  being a linear density distribution (measured in  $\mu\text{m}^{-1}$ ). Accordingly, the expression for the coupling constant  $g_{1D}$

here will read as  $g_{1D} = g'/4\pi a_{\perp}^2 = 2\hbar\omega_{\perp}a_s N$ , with  $a_{\perp} = \sqrt{\hbar/m\omega_{\perp}}$  (to further simplify notation,  $g_{1D}$  is used instead of  $g'_{1D}$ ).

Typical single dark soliton solutions for this nonlinear equation display the functional form [36]

$$\psi(z, t) = \sqrt{n_0} e^{-i(\mu/\hbar)t} \left[ \beta \tanh \left[ \beta \frac{(z - vt)}{\chi} \right] + i \frac{v}{c} \right] \quad (4)$$

for BEC clouds with a constant density  $n_0$ , where  $\mu = n_0 g$  is the chemical potential,  $c = \sqrt{\mu/m}$  is the so-called Bogoliubov speed of sound,  $\beta = \sqrt{1 - (v/c)^2}$  and  $\chi = \hbar/\sqrt{mn_0 g}$  is the coherence or healing length characterizing the soliton extension. The solution (4) represents a soliton propagating towards positive  $z$  with a speed  $v$  on a homogeneous background density  $n_0$ . As it can be readily inferred from Eq. (4), in the particular case  $v = c$ , the soliton will not be distinguishable from the background fluid [38]. Here, instead of a constant density, we analyze the case of space-limited condensates with an initial Gaussian profile, which somehow mimic the typical parabolic density profile that corresponds to a stationary solution inside a harmonic trap [7]. Note that solutions like (4) can be generated from the Gaussian ansatz by imprinting a phase shift to a part of the condensate leaving the other part unaffected [18]. Following this basic imprinting technique, the appearance of interference-type features in BECs can be understood as a sequential phase change, which allows us to identify the deeps in the cloud with a sequence of dark solitons, each with a shape analogous to Eq. (4). This will be made evident by means of the Bohmian analysis.

## B. Bohmian description

A central idea to hydrodynamics is that fluid diffusion can be monitored by means of streamlines, which provide us with information on the expansion, contraction, or rotation of the fluid. In a similar fashion, the Bohmian formulation of quantum mechanics or Bohmian mechanics renders a trajectory-based description of the evolution of quantum systems or, more strictly speaking, the diffusion of their probability density in the corresponding configuration space [24]. In its original version, either as formulated by Madelung in 1926 [39] or, later on, as postulated by Bohm in 1952 [40, 41], the main equations of motion are obtained after recasting the wave function in polar form (i.e., considering a nonlinear transformation from a complex-valued field to two real-valued fields) and then substituting it into the time-dependent Schrödinger equation. Proceeding the same way, i.e., substituting the polar ansatz (2) into Eq. (1), leads to the set of coupled hydrodynamic equations of motion

$$\frac{\partial \mathcal{N}(\mathbf{r}, t)}{\partial t} = -\nabla \cdot \mathbf{j}(\mathbf{r}, t), \quad (5a)$$

$$\hbar \frac{\partial \theta(\mathbf{r}, t)}{\partial t} + \frac{\hbar^2}{2m} (\nabla \theta)^2 + V_{\text{ext}}(\mathbf{r}) + g\mathcal{N}(\mathbf{r}, t) + Q(\mathbf{r}, t) = 0, \quad (5b)$$

where

$$\begin{aligned} \mathbf{j}(\mathbf{r}, t) &\equiv \frac{\hbar}{m} \mathcal{N}(\mathbf{r}, t) \nabla \theta \\ &= \frac{\hbar}{2mi} [\Psi^*(\mathbf{r}, t) \nabla \Psi(\mathbf{r}, t) - \Psi(\mathbf{r}, t) \nabla \Psi^*(\mathbf{r}, t)] \end{aligned} \quad (6)$$

is the quantum flux [42] associated with the process, which ensures the conservation of particles in the cloud by virtue of Eq. (5a). Equation (5b) displays the functional form of a Hamilton-Jacobi equation, although with the particularity that it contains the term

$$Q(\mathbf{r}, t) = -\frac{\hbar^2}{4m} \left\{ \frac{\nabla^2 \mathcal{N}(\mathbf{r}, t)}{\mathcal{N}(\mathbf{r}, t)} - \frac{1}{2} \left[ \frac{\nabla \mathcal{N}(\mathbf{r}, t)}{\mathcal{N}(\mathbf{r}, t)} \right]^2 \right\}, \quad (7)$$

which is the so-called Bohm's quantum potential [43]. As it can be noticed, unlike the motion described by a standard Hamilton-Jacobi equation, the presence of this additional term is going to induce a permanent coupling between the motion displayed by a single particle of mass  $m$  and a statistical ensemble of identical particles, specified by the density  $n$ .

From Eqs. (5) it is clear that individual trajectories or streamlines associated with the evolution of the quantum system described by (1) can be obtained either by postulating an equation of motion from (5b) [40, 43], in direct analogy with the classical counterpart,

$$\dot{\mathbf{r}}(\mathbf{r}, t) = \frac{\hbar}{m} \nabla \theta(\mathbf{r}, t), \quad (8)$$

or just, in a more natural way, by noting from the continuity equation (5a) that the quantum flux is typically associated with a local velocity field [24],

$$\mathbf{j}(\mathbf{r}, t) = \mathcal{N}(\mathbf{r}, t) \mathbf{v}(\mathbf{r}, t), \quad (9)$$

from which the same equation of motion follows,

$$\mathbf{v}(\mathbf{r}, t) = \dot{\mathbf{r}}(\mathbf{r}, t) = \frac{\mathbf{j}(\mathbf{r}, t)}{\mathcal{N}(\mathbf{r}, t)} = \frac{1}{m} \text{Re} \left\{ \frac{\hat{\mathbf{p}} \Psi(\mathbf{r}, t)}{\Psi(\mathbf{r}, t)} \right\}. \quad (10)$$

The last term, emphasizes the direct connection of this velocity vector field with the real part of the local value of the usual momentum operator  $\hat{\mathbf{p}} = -i\hbar\nabla$ . Hence, the trajectories obtained in this manner, i.e., from Eq. (10), are well-defined and are not in contradiction with standard quantum mechanics, where, in principle, one cannot appeal to the concept of trajectory in the configuration space, because of the uncertainty relation between position and momentum. Unlike classical trajectories, the swarms of trajectories obtained from Eq. (10) are constrained to obey a phase relation, according to which the corresponding momenta cannot be independent one another. This phase relation is precisely what we regard as coherence, which, in the present context, gives rise to the well-known Bohmian trajectory non-crossing rule: Bohmian trajectories cannot get across the same point at

the same time, this being a direct consequence from the single-valuedness of the local phase of quantum systems. Besides, it is worth stressing the fact that the equation of motion (10) not only establishes a direct link with usual transport equations, but also with the hydrodynamical description of Bose fluids earlier on proposed by Landau [44, 45].

### C. Trapping potential model

The confinement of neutral cold atoms in periodic lattices of reduced dimensions, which enables the investigation of BECs and their applications [46], including dark soliton dynamics [47], relies on the generation of periodic optical traps by counterpropagating laser beams [48, 49]. Thus, let us consider that a single atomic cloud, trapped in a harmonic potential, is adiabatically split up by applying an optical lattice a standing laser field. If the steepness of the harmonic trap is relevant in relation to the period of the optical lattice and the depth of its wells (see Fig. 1), and we assume an unbiased (or nearly unbiased) splitting of the cloud, we can assume that the BEC breaks into two, one half of each occupying a local minimum of the trap+lattice potential. To better understand the process in terms of the potential generated (for further details on these optical lattice potentials, see, for instance, Ref. [48, 49]), and hence the model here considered, let us consider that the confining potential along the  $z$ -direction consists of two contributions, namely,

$$V_{\text{ext}}(z) = V_{\text{trap}}(z) + V_{\text{latt}}(z), \quad (11)$$

where the harmonic trapping contribution reads as

$$V_{\text{trap}}(z) = \frac{1}{2}m\omega_z^2 z^2, \quad (12)$$

and the optical lattice as

$$V_{\text{latt}}(z) = V_0 \cos^2\left(\frac{\pi z}{\ell}\right). \quad (13)$$

Here we consider a  $^{85}\text{Rb}$  atomic cloud, with  $m = 1.44 \times 10^{-25}$  kg, so we have chosen typical experimental values [37, 50] for the parameters involved in these two contributions, in particular,  $f_z = 50$  Hz ( $\omega_z = 2\pi f_z \approx 314.2$  rad/s) and  $V_0/h = 850$  Hz (where  $h = 6.62607 \times 10^{-34}$  J·s is Planck's constant). Furthermore, with the purpose to discuss different dynamical behaviors, three values of the lattice constant,  $\ell$ , will be considered below:  $5.7 \mu\text{m}$ ,  $15 \mu\text{m}$ , and  $26 \mu\text{m}$ . To illustrate the overall effect, the two separate contributions as well as the combined potential (11) are displayed in Fig. 1 for  $\ell = 5.7 \mu\text{m}$ . The trap potential is denoted with the gray dashed line and the lattice potential with the blue dashed line, which their sum is represented with the black solid line. As it can be noticed, the activation of the lattice potential generates a barrier that is going to split up the atomic cloud basically into two parts. In a first approximation, each one of these parts can be assumed

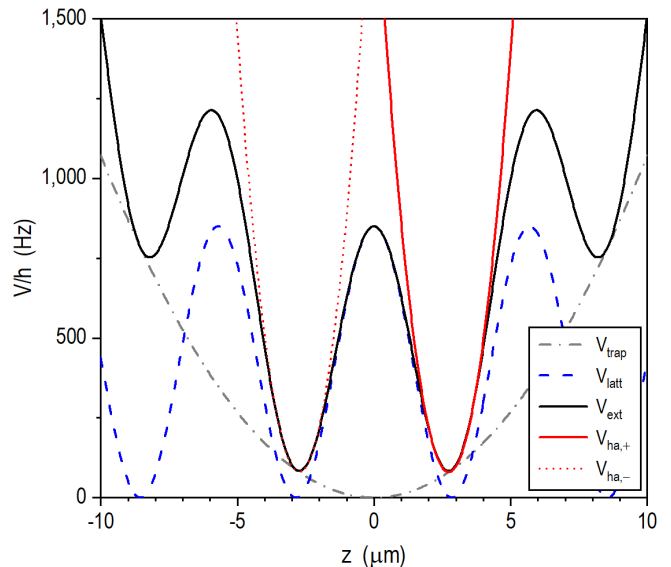


FIG. 1. External potential (solid black line) applied to split up a single atomic condensate and generate a coherent superposition of two condensates. The confining harmonic trap (dash-dotted gray line) here has a frequency  $f_z = 50$  Hz, while the lattice standing field (dashed blue line) has a period  $\ell = 5.7 \mu\text{m}$  and a potential barrier  $V_0/h = 850$  Hz. Each site or well on either side of the central barrier can be approximated by a harmonic potential (dotted and solid red lines) with an effective frequency  $f_{\text{eff}} \approx 245$  Hz (see text for details), which can be used to determine the initial ansatz in the simulations.

to be acted by a harmonic well with its frequency being determined by the lattice properties (barrier height and period). As it can readily be noticed, in a good approximation, for the case displayed in Fig. 1, these harmonic well can be approximated by the functional form

$$V_{\text{ha},\pm}(z) \approx V_{\text{trap}}(z_{\pm}) + \frac{1}{2}m\omega_{\text{eff}}^2(z - z_{\pm})^2, \quad (14)$$

with  $z_{\pm} \approx \pm\ell/2$  and

$$\omega_{\text{eff}} = \sqrt{\frac{2\pi^2 V_0}{m\ell^2}}. \quad (15)$$

From this expression, we can choose for the initial width of the Gaussian wave packet the one corresponding to the ground state of the harmonic oscillator, i.e.,

$$\sigma_{\text{eff}} = \sqrt{\frac{\hbar}{2m\omega_{\text{eff}}}}. \quad (16)$$

Of course, a more precise (though still approximated) form can easily be derived. However, for the purpose here, expression (15) suffices, since we are interested in releasing two coherently separated clouds from a fixed distance,  $\ell$ , which are assumed to be kept inside harmonic wells determined by the lattice potential (13) and not from the combined effect (11). Note that, as  $\ell$  increases,

the corresponding neighboring wells become shallow very rapidly, thus losing their appearance of a harmonic well, while the separation between the corresponding minima increases relatively slowly (below the value of  $\ell$ ).

#### D. Numerical details

In the calculations below, we have considered a cloud of 950  $^{87}\text{Rb}$  atoms, with scattering length  $a_s = 90 a_0 = 4.76$  nm [7]. With respect to the coupling constant  $g_{1\text{D}}$  that appears in the 1D GPE, we have considered a transverse trapping frequency value within the range indicated above, in particular,  $f_{\perp} = 408$  Hz. With this value,  $a_{\perp} = 534.5$  nm and  $g_{1\text{D}} = 2.45 \times 10^{-36}$  Kg·m<sup>3</sup>/s<sup>-2</sup>. Given the disparity of orders of magnitude involved in the different variables and parameters, in the calculations, for computational convenience, we have rescaled them in the 1D GPE (3). Specifically, first we have considered lengths in microns and times in milliseconds both in variables and in parameters (i.e.,  $\bar{x} = x/10^{-6}$  and  $\bar{t} = t/10^{-3}$ ), which are typical orders of magnitude for distances and times involved in experiments with condensates [37, 50], and then we have divided on both terms by  $\hbar$ , where the wave function, with dimensions of  $\text{length}^{-1/2}$ , is also rescaled ( $\bar{\psi} = \psi/10^3$ ). This leads to the following working functional form

$$i\hbar \frac{\partial \bar{\psi}}{\partial \bar{t}} = \left( -\frac{\hbar^2}{2\bar{m}} \frac{\partial^2}{\partial \bar{z}^2} + \frac{1}{2} \bar{m} \bar{\omega}_z^2 \bar{z}^2 + \bar{g}_{1\text{D}} |\bar{\psi}|^2 \right) \bar{\psi}, \quad (17)$$

with  $\bar{\hbar} = 1$ ,  $\bar{m} = 10^9 \times m/\hbar \approx 1.37$ ,  $\bar{\omega}_z = 10^9 \times \omega_z/\hbar \approx 0.36$ , and  $\bar{g}_{1\text{D}} = 10^9 \times g_{1\text{D}}/\hbar \approx 23.1895$ .

Without any loss of generality, we have assumed a Gaussian ansatz may fairly well describe the initial BEC density distribution in a qualitative manner. Note that we are interested here in the long-time dynamics rather than on the fine-grained structure of the short-living initial distribution, which will start getting the appropriate shape by virtue of the GPE nonlinear term. Thus, in one dimension, the initial wave functions are given by coherent superpositions of two identical Gaussian wave packets, with the functional form [51]

$$\begin{aligned} \psi(z) &= \psi_+(z) + e^{i\phi} \psi_-(z) \\ &\sim e^{-(z-z_+)^2/4\sigma_0^2} + e^{i\phi} e^{-(z-z_-)^2/4\sigma_0^2}, \end{aligned} \quad (18)$$

where  $z_{\pm}$  refers to the centroid position of each wave packet ( $z_{\pm} = \pm \ell/2$ ),  $\sigma_0$  is their width, which can be conveniently related to the lattice, as discussed in above, and  $\phi$  is a constant phase factor that can be imprinted on one of the condensates in order to analyze the influence of phase shifts. Note that, physically, this phase factor plays might the same role as the imprinting phase shift necessary to generate a dark soliton of the type described by Eq. (4), but also a Bohm-Aharonov-type shift between the two clouds. In both case, the same dynamical behavior is going to be observed in the evolution of the corresponding density distribution.

All initial states are numerically normalized to unity, so the analytical expression of the norm prefactor is irrelevant in (18) as it will depend on the grid size (see below). Apart from their simplicity, these ansätze are also convenient from an analytical viewpoint, since their time-evolution is given by an analytical expression both in free space and inside a harmonic potential in the linear case  $g_{1\text{D}} = 0$  [52], two scenarios that have been formerly considered in the literature [10]. This can be of some help to provide fair guesses regarding the choice of initial parameters and also to interpret the simulations.

Finally, regarding the time evolution, the split-operator method has been considered [53–55]. In brief, taking into account a small time step  $\delta t$ , the action of the evolution operator that actualizes the wave function from  $t$  to  $t + \delta t$  can be split up in three separate contributions,

$$\hat{U}(t) = e^{-i\hat{H}\delta t/\hbar} \approx e^{-i\hat{K}\delta t/2\hbar} e^{-i\hat{V}\delta t/\hbar} e^{-i\hat{K}\delta t/2\hbar}, \quad (19)$$

where  $\hat{K}$  denotes the kinetic part of the Hamiltonian and  $\hat{V}$  gathers the combined action of the external potential and the self-interaction nonlinear term. The kinetic contribution is solved in the momentum space, where  $\hat{K}$  is diagonal; to enhance the performance, the Fourier and inverse Fourier transforms are computed by means of the fast Fourier transform method [56], which is also advantageously used to evaluate the equation of motion in terms of the corresponding spectral decomposition (plane wave basis), and then to synthesize the Bohmian trajectories by numerically integrating it once the initial condition has been assigned [52]. The spatial part is solved by discretizing the wave function on an  $N$ -knot mesh, in particular, for the cases considered below, it suffices  $N = 1,024$ . Regarding the time evolution, a time step  $\delta t = 10^{-3}$  ms ensures good convergence in both cases (energy and norm are both preserved).

### III. RESULTS

#### A. Soliton formation with two freely released BECs

Let us first examine the formation process of dark solitons that arise after a BEC is first adiabatically split up by turning on the optical lattice, and then, after having separated it into two halves, the lattice is switched off, releasing the two portions again. Because of the harmonic trap, both parties will start moving against each other, which leads to the appearance of interference-like fringes after some time, even though the 1D GPE is a nonlinear equation and hence does not satisfy the superposition principle. In order to evaluate how the size of the two halves (measured in terms of the width  $\sigma_0$  of the corresponding wave packets) influences the appearance of such fringes (or dips in the full density distribution), let us consider that the condensates are let to freely evolve, i.e.,  $\omega_z \approx 0$ . Physically, this condition can be satisfied if the two condensates are relatively close one

another, so that they do not feel an important downhill acceleration prior to their interaction, and for times much smaller than a quarter of the classical period,  $T = 2\pi/\omega_z$ .

Taking into account the above conditions, it is expected that the two density distributions will essentially remain centered at the same position for the whole propagation, although their width will undergo an increase, larger as  $\sigma_0$  becomes smaller. In the linear case ( $g_{1D} = 0$ ), if  $\omega_z \approx 0$  and  $t \ll T/4$ , the time evolution of the wave packets  $\psi_{\pm}(z)$  is given by the expression [51]

$$\psi_{\pm}(z, t) \sim e^{-(z-z_{\pm})^2/4\sigma_0\tilde{\sigma}_t}, \quad (20)$$

where

$$\tilde{\sigma}_t = \sigma_0 \left( 1 + \frac{it}{\tau} \right), \quad (21)$$

with

$$\tau = \frac{2m\sigma_0^2}{\hbar} \quad (22)$$

being an effective time scale that determines how fast the wave packet spreads, since its spreading is given by

$$\sigma_t = |\tilde{\sigma}_t| = \sigma_0 \sqrt{1 + \left(\frac{t}{\tau}\right)^2}. \quad (23)$$

For instance, for  $\sigma_0$  given by Eq. (16), if  $\ell = 5.7 \mu\text{m}$ , we obtain  $\tau \approx 1.865$  ms, which means that only after a time much larger than this characteristic time scale, we will start observing an important overlapping between the two wave packets, and hence the appearance of interference features. Since the superposition principle can be applied in this case, the total wave function is simply

$$\psi(z, t) = \psi_+(z, t) + e^{i\phi}\psi_-(z, t), \quad (24)$$

and the density distribution will be

$$n(z, t) = n_+(z, t) + n_-(z, t) + 2\text{Re} [\psi_+(z, t)\psi_-^*(z, t)e^{-i\phi}], \quad (25)$$

with  $n_{\pm}(z, t) = |\psi_{\pm}(z, t)|^2$ . Taking into account Eqs. (20) and (21), the interference term in (25), which we will denote from now on as  $n_I(z, t)$ , reads as

$$n_I(z, t) \sim 2e^{-[z^2+(\ell/2)^2]/2\sigma_t^2} \cos\left(\frac{\hbar t \ell}{4m\sigma_0^2\sigma_t^2} z - \phi\right). \quad (26)$$

When the spread of the two Gaussian distributions is such that they overlap importantly, a rather suitable approximation for Eq. (25) is

$$n(z, t) \approx 4e^{-z^2/2\sigma_t^2} \cos^2\left(\frac{\hbar t \ell}{8m\sigma_0^2\sigma_t^2} z - \phi/2\right). \quad (27)$$

Accordingly, leaving aside the Gaussian envelope (determined by the Gaussian prefactor), the distance between any two consecutive interference maxima or minima is

$$\Delta z = \frac{8\pi m\sigma_0^2\sigma_t^2}{\hbar t \ell}, \quad (28)$$

which, for large  $t$  compared to  $2m\sigma_0^2/\hbar$  (but still much smaller than  $T/4$ ), simplifies to

$$\Delta z \approx \frac{2\pi\hbar t}{m\ell}. \quad (29)$$

Therefore, once the Gaussian distributions have undergone an important spread, the distance between consecutive fringes will not depend on the initial width  $\sigma_0$  of the wave packets, but only on the distance  $\ell$  between their centroids. Furthermore, notice that all interference maxima have the same width  $\Delta z$ . As for the phase difference between the two wave packets,  $\phi$ , it only causes a displacement of the fringes, producing a prominent dip at  $z = 0$  in the particular case  $\phi = \pi$ .

Based on the above analytical results, let us now investigate what happens in the nonlinear case, when  $g_{1D} \neq 0$ . In Fig. 2, in each panel, we show the density profile at three different times for an initially coherent superposition of two Gaussian BECs with different widths, but all of them with their centroids separated the same distance  $\ell = 5.7 \mu\text{m}$ . The value of  $\sigma_0$  increases from top to bottom in order to show the effect of the nonlinearity on the overlapping clouds (i.e., on densities that have not been efficiently separated). As it can be readily noticed, although  $\ell$  is the same in all cases, the nonlinear term gives rise to a different behavior regarding the appearance of interference-like traits. Thus, as  $\sigma_0$  increases, from top to bottom in the figure, we observe that the minima in the merging single condensate become less shallow, acquiring the shape of a slight perturbation on the general profile [see panel (b)]. It is also remarkable that, unlike the linear case, where the three cases should exhibit maxima and minima evenly spaced (at least in those cases with a high visibility, which here correspond to small  $\sigma_0$ ), the central maximum is wider than the side ones, although of the order of the value rendered by Eq. (29), which here is about  $5 \mu\text{m}$  for  $t = 5$  ms [in agreement with what we can observe in Fig. 2(a), black curve].

The dynamics giving rise to the appearance of the interference-like traits discussed above can be better understood by inspecting the density plots shown in Fig. 3, where the evolution of the three superpositions is monitored until  $t = 3$  by means of Bohmian trajectories (see yellow solid lines superimposed in each panel). For a better understanding of the BEC hydrodynamics, equidistant initial conditions have been considered, spanning a region well beyond very low values of the density. Thus, comparing these trajectories with those associated with a linear case (see, for instance, [24]), here there is a more abrupt turn outwards of the trajectories (flow) once the two clouds start overlapping, although at a qualitative level in both the linear case and the nonlinear one similar trends are observable. By inspecting the upper row in Fig. 3, from left to right, we observe how the interference-like structure gets diluted as the initial overlapping of the two condensates becomes larger (with increasing  $\sigma_0$ ). On the other hand, the lower row, which shows the density plot of the evolution in time of the (drift) velocity field

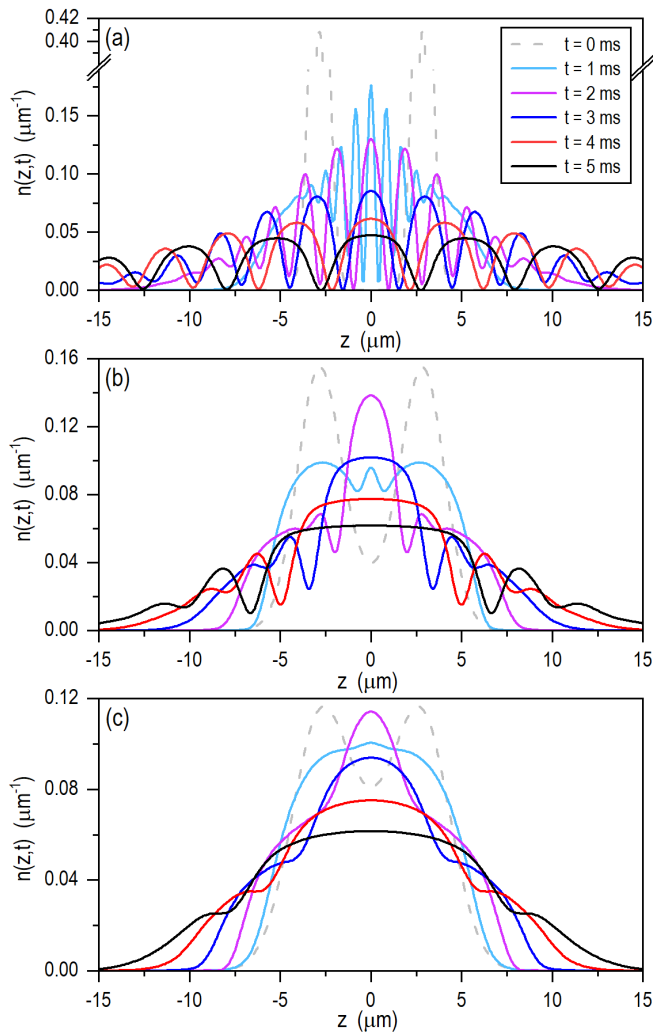


FIG. 2. Density distribution at various times (see color legend in upper panel) illustrating different stages of the dynamical evolution of a coherent superposition of two identical Gaussian condensates with an initial peak-to-peak separation  $\ell = 5.7 \mu\text{m}$ . In all panels, the width of the initial Gaussian is specified by the expression  $\sigma_0 = r\sigma_{\text{eff}}$ , where  $\sigma_{\text{eff}} \approx 0.49 \mu\text{m}$  is specified by Eq. (16) and  $r$  is a parameter related to the initial (at  $t = 0$ ) overlapping between the densities  $n_+$  and  $n_-$  that appear in Eq. (25). Here, this overlapping is measured in terms of the ratio  $S \equiv n(0,0)/n_{\text{max}}(z_{\pm},0)$ , where  $n(0,0)$  is Eq. (25) evaluated at  $z = 0$  and  $n_{\text{max}}(z_{\pm},0)$  is the maximum value reached by  $n(0,0)$  (at  $z_+$  or  $z_-$ ). Thus, from top to bottom: (a)  $r = 1$  and  $S \approx 0$ , (b)  $r = 2.5$  and  $S \approx 0.26$ , and (c)  $r = 3.2$  and  $S \approx 0.70$ .

provides us with an alternative picture for such a behavior. Although initially this field is zero, because there is no local variation of the phase in the initial wave function, for low values of  $\sigma_0$ , after a very short time, the velocity field acquires important negative (dark shading, from gray to black; see shading code in the r.h.s. legend) and positive (faint shading, from gray to white) values, dividing the space dynamically. A first division is related to the symmetry line, at  $x = 0$ , which will remain

for all times; accordingly, trajectories related to one of the clouds cannot penetrate the region determined by the other cloud, and vice versa. This happens for all values of  $\sigma_0$  and is related to the so-called non-crossing property of Bohmian trajectories [51], which arises from the single-valuedness of the underlying velocity field [24]. A second division is connected to the (space-dependent) phase acquired by each individual cloud, which in the linear case is given by (20), and that makes the associated trajectories to move in opposite directions, thus causing their dispersion and hence the widening of the density distribution. Now, in the case of low  $\sigma_0$  values, there is a longer range of interaction between the two clouds, which results, at later times, on solitons with a higher visibility. Note in Fig. 3(d) that, between  $t \approx 0.1$  ms and  $t \approx 1.2$  ms, the region between the centers of the two condensates is dominated by two intense velocity fields with opposite values. When  $\sigma_0$  increases and the overlapping is more important, such a region decreases and gets smoother, thus leading to fainter interference minima, even though at later times, as seen in Fig. 2(b), they become more apparent. However, beyond certain values of  $\sigma_0$ , the active region between the two clouds becomes irrelevant and interference traits blur, as seen in Fig. 3(f) [see also Fig. 2(c)].

Unlike the linear case, though, a series of kinks appear in the trajectories as they become abruptly deflected outwards (in the linear case, such deflection takes place more gradually). Typically, these kinks appear around nodes of the wave function in the linear case, where the velocity field undergoes fast changes in the form of positive or negative spikes (see, for instance, Ref. [24]). A close inspection at the lower row panels in Fig. 3 shows that also in the nonlinear case this is the case, since a series of sudden and highly localized changes in the velocity arise in the form of chains on both sides and for all values of  $\sigma_0$ . These features, which are very prominent in the plots of the velocity fields, because any sudden phase change affects importantly the local velocity, can also be found in the density plots of the probability density (not shown here), but only if one considers its logarithmic representation, since they take place in regions where the density values are already very low. On the contrary, if we launch trajectories with initial conditions in the regions where the initial density  $n(z,0)$  is already negligible, they will be able to detect these important phase variations even if the density values are very low. This is precisely where the strength of the trajectory or, analogously, velocity field method relies on: phase changes in regions with negligible densities can be immediately detected, because of the tight connection between phase correlation and Bohmian trajectory.

Given the high sensitivity of the trajectories to phase changes, they can also be used to detect other phase-based effects. Consider, for instance, an Aharonov-Bohm type shift, like the one induced on the interference of two coherent electron beams acted by a shielded magnetic field, as reported by Tonomura *et al.* [57]. The action of



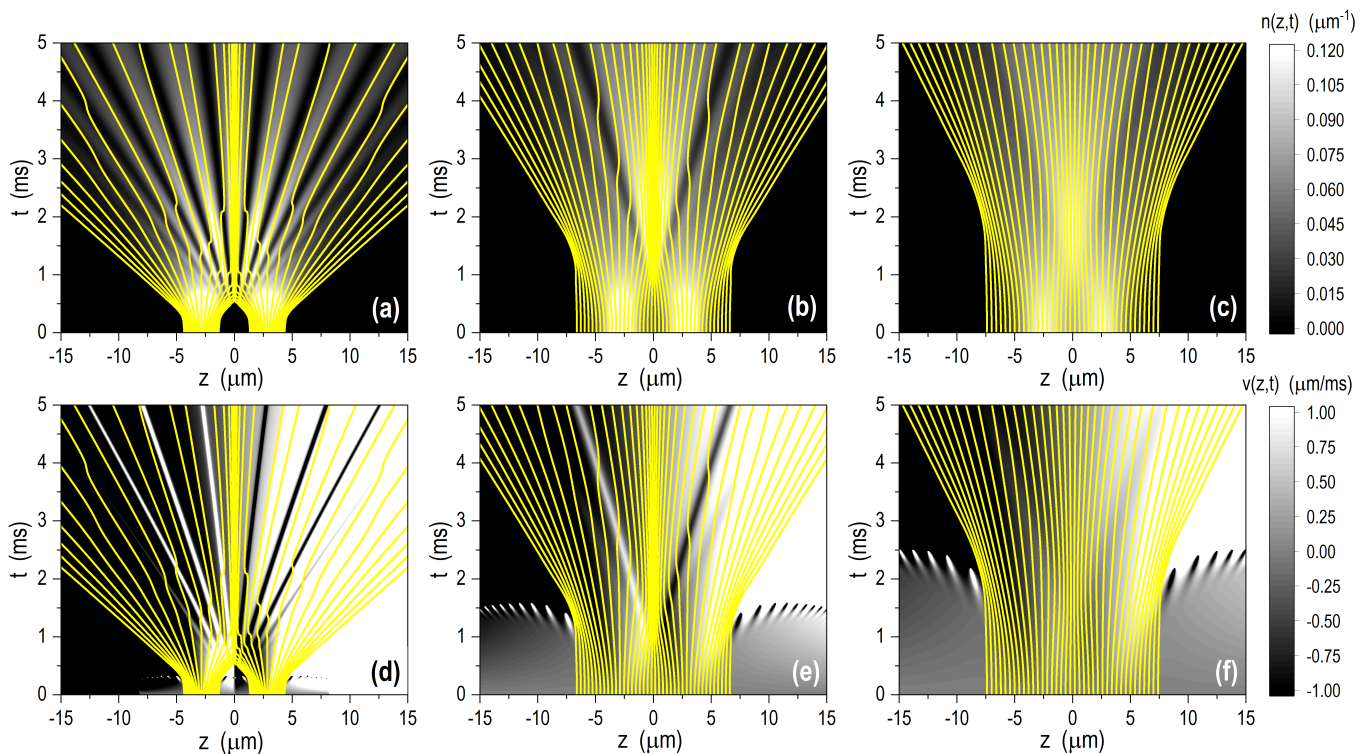


FIG. 3. Time-evolution of the BEC density distribution (top row) and its associated velocity field (lower row) for the three cases displayed in Fig. 2: (a/d)  $r = 1$ , (b/e)  $r = 2.5$ , and (c/f)  $r = 3.2$ . The shading code to the right denotes the scale considered, from black for the lowest values of the quantities displayed to white for the highest values considered. For a better visualization and comparison, the density distributions have been truncated to  $0.12 \mu\text{m}^{-1}$ , while the velocity field ranges within  $\pm 1 \mu\text{m}/\text{ms}$ . To illustrate the flux dynamics, in all plots sets of 50 Bohmian trajectories (solid yellow lines) are superimposed, with their initial conditions covering homogeneously regions of the density distribution larger than 0.5% its highest value. (For a better visualization of only the density plots, they are provided without the sets of trajectories in the form of Supplemental Material; see Fig. S3.)

the shielded field can be simulated by simply shifting the relative phase between the electron beams. In the linear case, a trajectory simulation of this fundamental result was already provided by Philippidis *et al.* [58]. To some extent, due to the linearity of Schrödinger's equation, this is an expected result, since the phase factor is going to directly appear in the argument of the cosine that rules the interference term (26). In the nonlinear case, though, considering  $\phi \neq 0$  in (24) does not warrant a priori a subsequent effect at later times. However, as in the counter-intuitive case of finding an interference-like behavior, also such an additional phase difference between the two merging clouds is going to have an important manifestation in the behavior of the interference traits, as shown in Figs. 4(a) and (d), for  $\sigma_0$  with  $r = 1$  and  $r = 3.2$ , respectively, and where in both cases  $\phi$  takes the values  $-\pi/2$  (blue solid line),  $\pi/2$  (green solid line), and  $\pi$  (red solid line). To compare with, the case  $\phi = 0$  (gray dashed line) has also been added in each case. As it is seen in Fig. 4(a),  $\phi$  only produces a shift of the solitons, leftwards if it is negative and rightwards if it is positive; in the case  $\phi = \pi$ , what we observe is that solitons appear in the positions corresponding to the maxima of the

density distribution, and vice versa, which is due to the fact that, at  $t = 0$ , the density has to be cancel out at  $z = 0$ , according to the relation

$$\begin{aligned} n(0,0) &= 2n_{\pm}(0,0) + 2n_{\pm}(0,0) \cos \phi \\ &= 4n_{\pm}(0,0) \cos^2(\phi/2) \end{aligned} \quad (30)$$

(note that, at  $z = 0$ , both  $n_{-}$  and  $n_{+}$  acquire the same value, so it does not matter which one is chosen). Note that, even if this relation is not satisfied anymore along the evolution of the condensate, because of the lack of linearity of the 1D-GPE, the conservation of the flux constrains (made evident through the Bohmian trajectories) implies that  $n(0,t)$  must be zero at any subsequent time. This is precisely what we observe in Fig. 4(a), where  $t = 5$  ms and despite of initially having two well separated clouds. This effect, though, is more interesting in the case of overlapping condensates. As seen in Fig. 4(d), although for  $\phi = 0$  no solitons emerge, as  $\phi$  is increased (or decreased towards negative values), the start emerging, because the overlapping between the two clouds is going to increase. The most remarkable case takes place for  $\phi = \pi$ : although the two clouds are wide enough to spatially overlap, the appearance of a  $\pi$ -phase



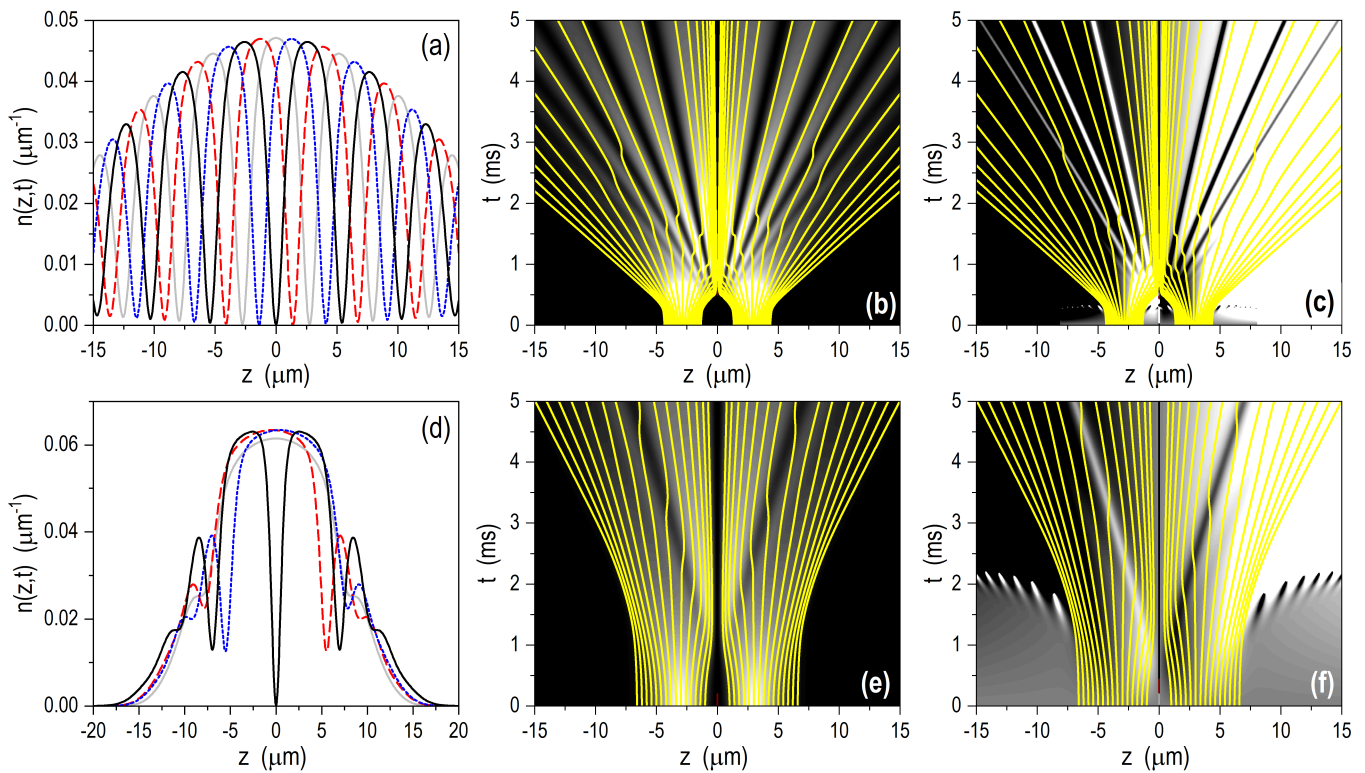


FIG. 4. Effect of the phase difference  $\phi$  on the dynamics exhibited by a coherent superposition of two condensates with identical Gaussian distributions, with peak-to-peak distance  $\ell = 5.7 \mu\text{m}$  and width  $\sigma_0 = r\sigma_{\text{eff}} \approx 0.49r \mu\text{m}$ . In the upper row, results for  $r = 1$ : (a) density profiles at  $t = 5 \text{ ms}$  for  $\phi = 0$  (solid gray line),  $\pi/2$  (dashed red line),  $\pi$  (solid black line), and  $-\pi/2$  (dotted blue line); (b) and (c) density plots showing the time evolution of the density distribution and the velocity field, respectively, together with the corresponding Bohmian trajectories superimposed (solid yellow lines) for  $\phi = \pi$ . In the lower row, the same for  $r = 3.2$ . The shading code for panels (b), (c), (d), and (f) is the same as in Fig. 3. (For a better visualization of only the density plots, they are provided without the sets of trajectories in the form of Supplemental Material; see Fig. S4.)

difference between both will make the initial density to vanish at  $z = 0$ , thus generating two initially separate distributions. As time proceeds, the same interference-like phenomenon will then be observed, which eventually leads to the appearance of solitons, just like in the case for  $\phi = 0$ , although in a lesser number. The density plots in panels (b) and (e) for the density distribution, or in panels (c) and (f) for the local velocity field, provide us with a clear picture on how this interference process mediated by a initial phase difference takes place, and how the flux, described by means of Bohmian trajectories, shows the appearance of the corresponding dark solitons by a recast of the density in some regions, while quickly avoids others (those occupied by the solitons). These numerical simulations are in good agreement with those in Ref. [37], where a potential energy difference of the initial condensates is used to induce the phase difference.

## B. Soliton formation from two BECs released in a harmonic trap

Let us now consider the case where the effects of the harmonic trap are important and the two clouds are let to evolve inside, each released from an opposite site of the potential. As before, the distance between their centroids is  $\ell$ . Regarding the initial width, also as before, we make some considerations based on the linear case. Thus, when a Gaussian wave packet is released inside a harmonic well with frequency  $\omega_z$ , if its initial width is  $\sigma_0^2 = \hbar/2m\omega_z$ , the time evolution of the wave function is given by [59]

$$\psi(z, t) \sim e^{-(z-z_0 \cos \omega_z t)^2/4\sigma_0^2 - i\omega_z t/2} \times e^{-im\omega_z(4zz_0 \sin \omega_z t - z_0^2 \sin 2\omega_z t)/4\hbar}, \quad (31)$$

which shows that the width of the probability density remains constant in time. This means that the corresponding Bohmian trajectories [obtained from the phase of Eq. (31)] will exhibit a recurrent oscillatory motion, according to the equation

$$z(t) = z(0) - z_0 + z_0 \cos \omega_z t, \quad (32)$$

which also shows that the trajectories are parallel one another. Otherwise, if the initial width is not constrained to the above value, the wave packet undergoes a sort of "breathing", with its width oscillating as it moves from one turning point to the opposite one, and vice versa. Consequently, the corresponding trajectories will not be parallel, but will separate from the central one (the one with its initial condition coinciding with the position of the initial centroid of the wave packet) and can back again periodically. If a coherent superposition of two of such wave packets is considered, each one located on opposite turning points initially, and regardless of the value of  $\sigma_0$ , the associated trajectories will undergo a bounce backwards whenever they reach the center of the potential, as they must satisfy the above mentioned non-crossing rule [51, 52].

In the present case, given that the two initial wave packets arise from a former confinement in the wells formed by the lattice sites, we are going to assume that both correspond to the ground state of the corresponding approximated harmonic potentials. Thus, the superposition will take the form of (18), with  $z_{\pm} = \pm\ell/2$  and  $\sigma_0^2 = \hbar/2m\omega_{\text{eff}}$ . As for the effective frequency  $\omega_{\text{eff}}$ , we will consider Eq. (15), which decreases with  $\ell^{-1}$ , since increasing  $\ell$  implies wider and wider effective harmonic wells. Here we are going to consider the same three values for  $\ell$ , which make  $f_{\text{eff},1} = 245.3$  Hz for  $\ell = 5.7$   $\mu\text{m}$ ,  $f_{\text{eff},2} = 93.2$  Hz for  $\ell = 15$   $\mu\text{m}$ , and  $f_{\text{eff},3} = 53.8$  Hz for  $\ell = 26$   $\mu\text{m}$ , with  $f_{\text{eff}} = \omega_{\text{eff}}/2\pi$ . If the nonlinear case shows some similarities with the linear one, we should expect the appearance of different dynamical behaviors depending on whether  $f_{\text{eff}}$  approaches the value of  $f_z = 50$  Hz or diverts from it. Actually, taking into account that the spreading of the wave packet under linear conditions, given by Eq. (23), is ruled by the effective width at  $t = T/4$ ,  $\sigma_{\pi/2} = \hbar\omega_{\text{eff}}/2m\omega^2$ , there will be an additional constraint involved in the process. Thus, we have  $\sigma_1 = 2.39$   $\mu\text{m}$  for  $\ell = 5.7$   $\mu\text{m}$ ,  $\sigma_2 = 1.47$   $\mu\text{m}$  for  $\ell = 15$   $\mu\text{m}$ , and  $\sigma_3 = 1.19$   $\mu\text{m}$  for  $\ell = 26$   $\mu\text{m}$ , to be compared with the width corresponding to a coherent wave packet,  $\sigma_c = \hbar/2m\omega^2 = 1.08$   $\mu\text{m}$  (with  $f_z = 50$  Hz).

In Fig. 5 we can observe the three possible dynamical scenarios that can take place inside the harmonic trap depending on the value of  $\ell$ , which rules both the separation between the two clouds (distance between two neighboring sites) and their initial width (related to the approximated harmonic well). Following a linear dynamics, we observe that, for  $\ell = 5.7$   $\mu\text{m}$ , the initial width is quite different from the width expected for a coherent state in the harmonic trap. Hence, it is expected that it will undergo the above mentioned "breathing". In Fig. 5(a) we observe that, effectively, because the width of the initial clouds do not match that of a coherent wave packet, they undergo an important spreading, giving rise to the appearance of interference-like traits at about  $t = T/4$ . As it is shown by means of the superimposed trajectories, this structure repeats a few times until it starts getting blurred precisely at the times where one would expect a

revival of the initial state, at about multiples of half the period. A closer inspection shows that this blurring consists of a mesh of nodes that, as time proceeds, spread all over the place that should be occupied by interference traits, which are pushed beyond them, as it can be seen in the subsequent expansions after 30 ms. The messy behavior of the trajectories indicates that the density between two consecutive solitons is being transferred from the most external parts of the condensate to the innermost ones. It is this effective transfer that eventually leads, when it gets in contact with the flux associated with the core part of the density, to the appearance of the web of nodes. A different behavior is observed for  $\ell = 26$   $\mu\text{m}$ , as it is shown in Fig. 5(c). In this case, the effective frequency is pretty close to the frequency of the harmonic trap, so the initial width of the clouds is close to that of coherent wave packets. Hence, the first stages in the evolution of the clouds are analogous to those that can be observed in the linear case, with the typical bounce backwards of the trajectories at  $t = T/2$ . It is precisely in this region where a series of aligned solitons arise, remaining for longer times, although the nonlinearity causes that the clouds sent towards the turning points will increase their width. These two behaviors are pretty similar to the Young-type and collision-type interference process that can be found when we are dealing with the linear evolution of a coherent superposition of two wave packets [51]. In between, as seen in Fig. 5(b), we observe a transition dynamics that keeps features from the two regimes.

If we look at the corresponding velocity plots instead, displayed in Fig. 6, we observe a rather enlightening picture for the dynamical behavior exhibited by the density distribution. As seen in Fig. 6(a), for early times, the density is acted by a velocity field that is relatively homogeneous, with positive (faint shading, from gray to white; see shading code in the r.h.s. legend) and negative values (darker shading, from gray to black). In those regions where the velocity field acquires positive values, the trajectories (flux) are driven upwards, towards positive  $z$ , while negative values lead the trajectories downwards, along the negative  $z$ -direction. At about  $t = 5$  ms, a series of grayish bands, representing velocity values around 0, starts emerging, separated by other sharp negative and positive velocity regions; the trajectories avoid these regions, accumulating along the grayish "valleys", where the values of the velocity are moderate or even negligible. At this time, there is also a broad expansion of the set of trajectories, as it corresponds to wave packets that feel a mild effect from the confining potential; the weaker the interaction the larger the spread range, as it happens in a linear case, in a typical Young-type two wave-packet collinear interaction [51]. Afterwards, because of the action of the confining potential, the swarm of trajectories starts gathering again guided by an exchange of the sign of the velocity field (the positive region becomes negative, and vice versa), until an approximate revival of the initial density is observed at  $t \approx 10$  ms, which corresponds to nearly half the period of the harmonic poten-

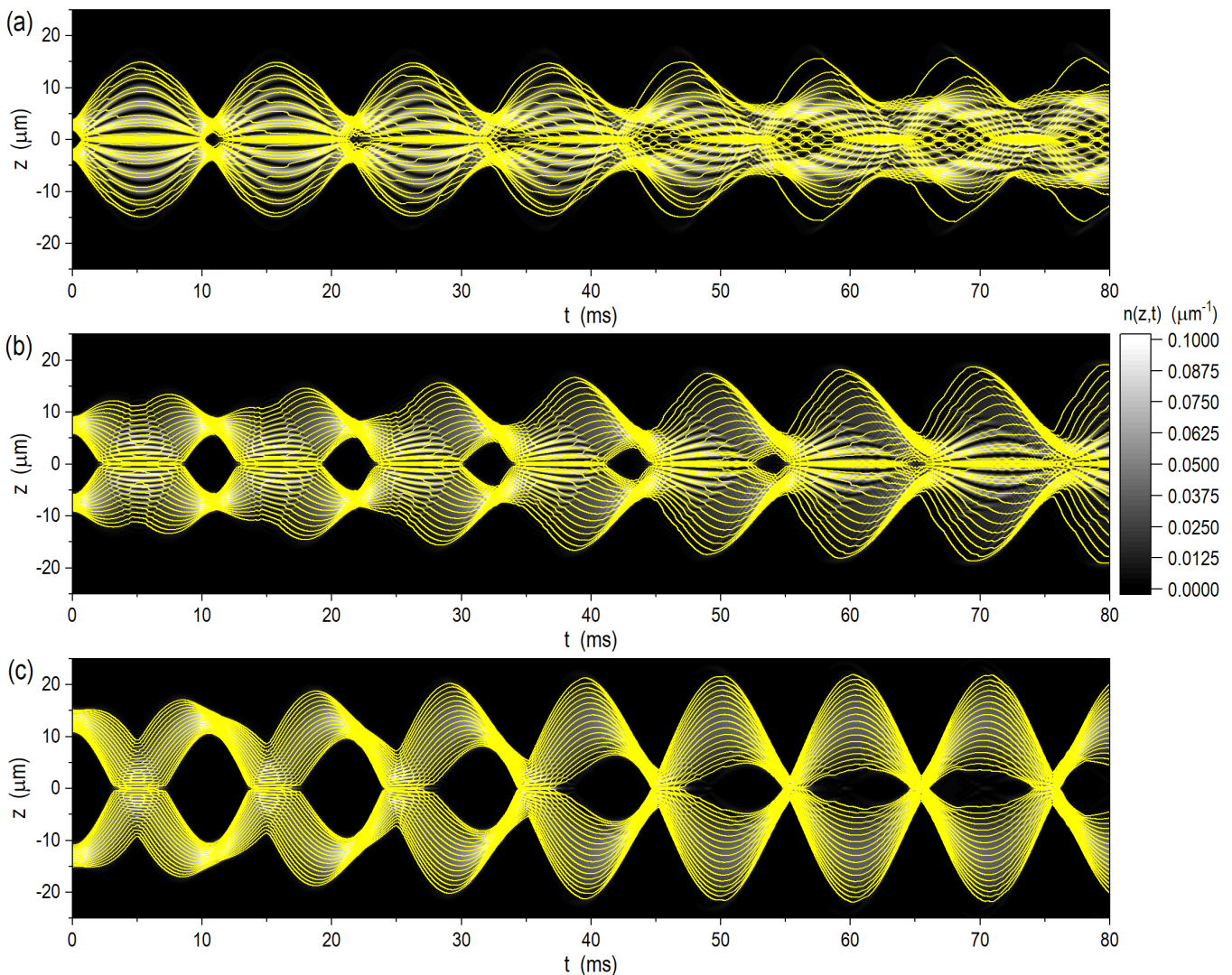


FIG. 5. Contour plots showing the time evolution of the density distribution associated with three initial superpositions with peak-to-peak distances: (a)  $\ell = 5.7 \mu\text{m}$ , (b)  $\ell = 15 \mu\text{m}$ , and (c)  $\ell = 26 \mu\text{m}$ . The shading code is defined on the right; the distributions have been truncated to  $n_{\text{max}} = 0.1 \mu\text{m}^{-3}$  in all cases for a better visualization. Sets of Bohmian trajectories (solid yellow lines) with homogeneously distributed initial conditions are superimposed in order to illustrate the local aspects exhibited by the condensate dynamics. In all cases the frequency of the harmonic trap is  $f_z = 50 \text{ Hz}$ . (For a better visualization of only the density plots, they are provided without the sets of trajectories in the form of Supplemental Material; see Fig. S5.)

tial,  $T = 20 \text{ ms}$ . Note that, because the two condensates are identical, the trajectories cannot cross the symmetry axis  $x = 0$ , and hence the repetition of the pattern takes place in half a cycle under linear propagation conditions [51]. The same trend is observed at subsequent times, although there is a degradation of the neat alternating structure of the velocity field, which consequently leads to a blurring of the region where the interferential valleys appear. Thus, because of the presence of the nonlinearity, the two well-defined dynamical regimes, specified by regions of opposite velocity fields and regions with alternate interference bands, start mixing, generating new interferential patterns [see Fig. 5(a)]. As it can be seen, the trajectories are very sensitive to these structures, since

they always try to avoid very quickly regions with low density, associated with sudden changes in the velocity field.

In the opposite case, when the two wave packets start quite far apart one another, as it is seen in Fig. 6(c), the regions with opposite velocity field values are more clearly defined and their preservation remains for a longer time. However, the intermediate interference region with low velocity values is almost negligible, as it would correspond to a situation analogous to a collinear collision of two wave packets in a linear regime [51]. In such situations, although the trajectories cannot cross the symmetry line, it can be noticed that, on average, they behave like moving along the trajectory of a classical harmonic



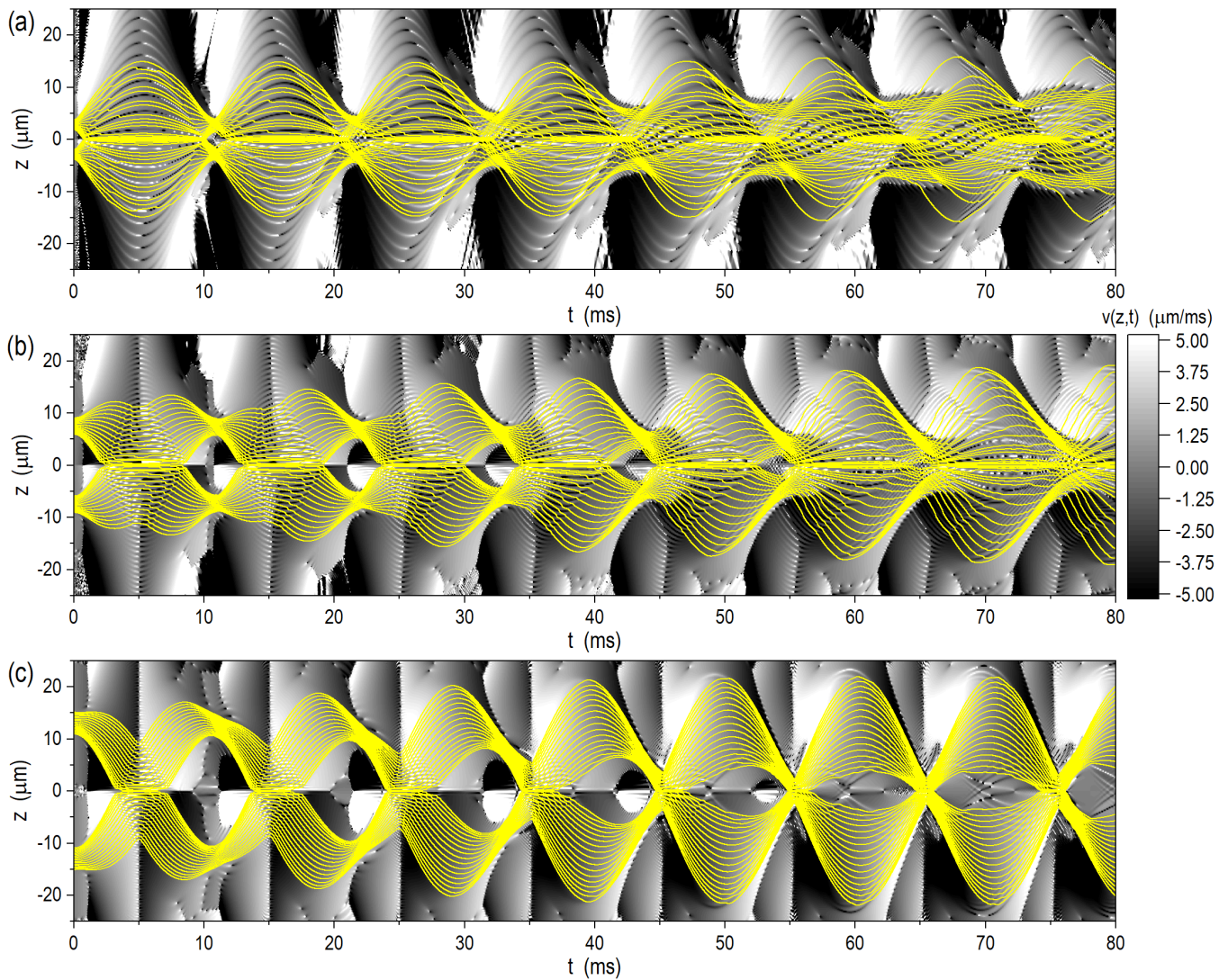


FIG. 6. Contour plots showing the time evolution of the velocity field associated with the three initial superpositions considered in Fig. 5, with peak-to-peak distances: (a)  $\ell = 5.7 \mu\text{m}$ , (b)  $\ell = 15 \mu\text{m}$ , and (c)  $\ell = 26 \mu\text{m}$ . The shading code is defined on the right; velocity values have been constrained to the range  $\pm 5 \mu\text{m/ms}$  in all cases for a better visualization. Sets of Bohmian trajectories (solid yellow lines) with homogeneously distributed initial conditions are superimposed in order to illustrate the local aspects exhibited by the condensate dynamics. In all cases the frequency of the harmonic trap is  $f_z = 50 \text{ Hz}$ . (For a better visualization of only the density plots, they are provided without the sets of trajectories in the form of Supplemental Material; see Fig. S6.)

oscillator. Of course, the presence of the nonlinearity introduces the corresponding deviations, but still we can perceive this type of back and forth motion along time. In those regions where the two wave packets overlap (at about a quarter of a period, for instance), the trajectories bounce backwards, but there is an effective transfer of the state of motion that they describe from the upper swarm to the lower one, and vice versa, which provides us with a certain sense of flow continuity. Note that this happens by virtue of the quick velocity flipping at the instant where the two sets of trajectories reach their maximum proximity, even at any later time, when the topology displayed by both swarms has nothing to do

with the initial swarms.

The repetitive behavior of the velocity field can then be used in a profitable manner to determine the precise times at which maximum fringe visibility is expected in the merging of the two condensates by simply determining the time at which the velocity field flips take place. Equivalently, the same can be done from the times at which the sets of trajectories undergo the bounce backward, something that cannot be unambiguously done in the case of initially close wave packets beyond few periods. This fact is illustrated in Fig. 7, where the density distribution for  $\ell = 5.7 \mu\text{m}$  [part (a)] and  $\ell = 26 \mu\text{m}$  [part (b)] has been plotted for some times at which there

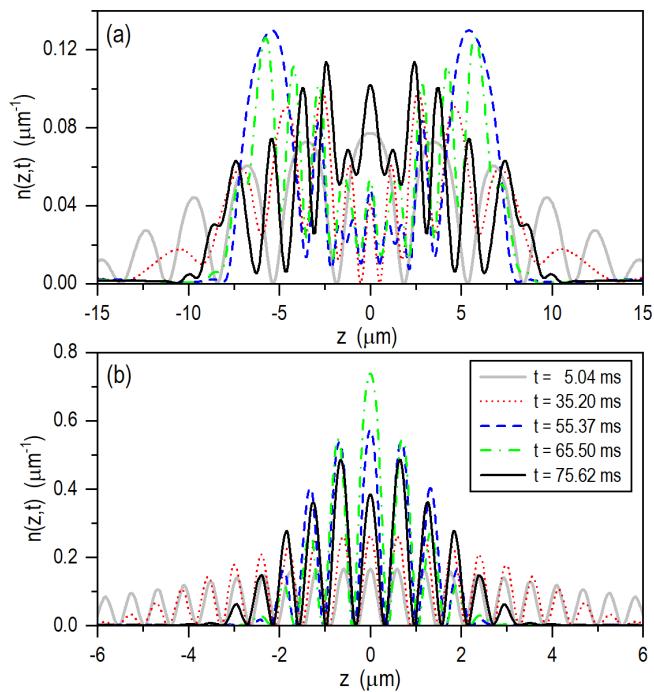


FIG. 7. Density distribution at different times for coherent superpositions of two condensates inside a harmonic trap with  $f_z = 50$  Hz and peak-to-peak distances: (a)  $\ell = 5.7 \mu\text{m}$  and (b)  $\ell = 26 \mu\text{m}$ . As it can be read in the legend inserted in the lower panel, the times considered in both cases are:  $t = 5.00$  ms (solid gray line),  $t = 35.20$  ms (dotted red line),  $t = 55.37$  ms (dashed blue line),  $t = 65.50$  ms (dash-dotted green line), and  $t = 75.62$  ms (solid black line).

is a sudden velocity flip in the case displayed in Fig. 6(c). For  $\ell = 5.7 \mu\text{m}$ , we observe that the series of dark solitons emerged by interference disappears very quickly. For  $\ell = 26 \mu\text{m}$ , however, although the ranged occupied by the series of dark solitons decreases with time, they still keep showing up with almost the same width and period. Accordingly, we find that the process of dark soliton generation by merging two condensates, of much interest for BEC interferometry, is thus more robust as such condensates are more distant initially, i.e., as the period of the lattice becomes larger.

#### IV. CONCLUDING REMARKS

The dynamics involved in matter-wave interferometry with condensates are known to be well described by the mean-field theory in terms of the GPE. Despite of the nonlinearity of the GPE, the coherent merging of two formerly split up condensates gives rise to the appearance of interference-type structures, where the minima can be identified with dark solitons, which, in turn, arise as a consequence of the atom-atom repulsion (implicitly included in the GPE nonlinear term). In order to provide an alternative perspective on the dynamical processes where these structures arise, here different scenarios have been analyzed within the hydrodynamical framework of

Bohmian mechanics. Thus, the velocity field associated with local phase variations of the wave function (order parameter) and the flux trajectories that evolve accordingly render a different view and understanding of the appearance of interference-type features. To stay close to known situations, in particular, here we have considered cases previously investigated both numerically and experimentally in the literature, characterized by the appearance of arrays of dark solitons [37, 50]. As it is shown, although the process somehow resembles the emergence of interference fringes in the standard linear case (i.e., in a typical Young-type experiment), the presence of nonlinearities invalidates the direct application of the superposition principle and, therefore any explanation or interpretation based on it.

Following the current (mean field) hydrodynamical description, it is noticed that the gradual appearance of the dips in the condensate density distribution, which are commonly identified with interference minima, can be identified with the formation of dark solitons, because they are associated with a phase difference analogous to that involved in the imprinting technique that provokes the generation of single dark solitons in a homogeneous cloud. In the current case, instead of only having the usual step-type phase variation that is imprinted on the condensate, there is an alternating (almost periodic) succession of such step-type structures, which are detected within our approach by computing the local velocity field (directly related to the gradient of the phase) and the flux (Bohmian) trajectories. At such positions, the velocity field undergoes a sudden and prominent increase or decrease, which it remains nearly constant between any two of these “kicks”. The presence of these localized changes in the velocity provides us with a clue on where a dark soliton has formed. Furthermore, as a consequence, in these regions the flux feels a sudden acceleration, which provokes fast turns in the corresponding trajectories. This thus forces the trajectories to jump from a given spatial region of nearly zero acceleration to a neighboring one, while leaving empty the region where they undergo the boost remains lowly populated. This process, with flux trajectories getting accumulated in certain regions, explains the inhomogeneity in the intensity distribution, with a structure resembling that of an interference pattern, although the dynamical origin is different. This behavior has been observed both in freely released condensates and also in condensates released inside a harmonic trap.

In relation to the above comment, in the case of freely released condensates, we have seen that by simply adding a phase difference between the two condensates that constitute the initial superposition state automatically leads to the appearance of soliton-type features. Of course, this can be expected, because the process is basically the same as the imprinting technique used to generate dark solitons in a single cloud, even though here we start with two spatially separated clouds. However, note that, on the other hand, this situation also resembles that of

the Aharonov-Bohm effect, where a local phase change in one of the two branches of the wave function leads to a measurable shift of the interference features. The representation in terms of velocity fields and trajectories allow us to detect the effect generated by these initial phase differences between the two clouds. In particular, for  $\phi = \pi$ , a deep dark soliton will emerge at the center in the case of identical initial clouds, This region will be avoided by the corresponding flux trajectories, which will accumulate either on one side or the other of this singular region, but never approaching the half point, contrary to what happens with  $\phi = 0$ .

Finally, in the case of condensates inside a harmonic trap, we have also seen that a knowledge of the velocity field or the corresponding flux trajectories has an intrinsic practical interest, as it allows us to determine in a more accurate manner time scales ruling the conden-

sate dynamics. The fact that the velocity field displays sudden changes (or the trajectories exhibit clear turns) constitute an important advantage against simply considering an inspection of the time evolution of the density distribution, since such changes are quite unambiguous spatially (as well as the trajectory turns). Additionally, from the interferometric point of view, this analysis also offers valuable information about why the superposition of the two condensates shows a remarkable dependence on the releasing position or how long we can wait until observing a degradation of the oscillatory dynamics.

#### ACKNOWLEDGMENTS

Financial support from the Spanish Agencia Estatal de Investigación (AEI) and the European Regional Development Fund (ERDF) (Grant No. PID2021-127781NB-I00) is acknowledged.

- 
- [1] M. R. Andrews, C. G. Townsend, H.-J. Miesner, D. S. Durfee, D. M. Kurn, and W. Ketterle, Observation of interference between two Bose condensates, *Science* **275**, 637 (1997).
- [2] W. Ketterle, Nobel lecture: When atoms behave as waves: Bose-Einstein condensation and the atom laser, *Rev. Mod. Phys.* **74**, 1131 (2002).
- [3] J. Javanainen and M. Wilkens, Phase and phase diffusion of a split Bose-Einstein condensate, *Phys. Rev. Lett.* **78**, 4675 (1997).
- [4] J. Javanainen and S. M. Yoo, Quantum phase of a Bose-Einstein condensate with an arbitrary number of atoms, *Phys. Rev. Lett.* **76**, 161 (1996).
- [5] F. Dalfovo, S. Giorgini, L. P. Pitaevskii, and S. Stringari, Theory of Bose-Einstein condensation in trapped gases, *Rev. Mod. Phys.* **71**, 463 (1999).
- [6] L. P. Pitaevskii and S. Stringari, *Bose-Einstein condensation and superfluidity*, Vol. 164 (Oxford University Press, 2016).
- [7] C. J. Pethick and H. Smith, *Bose-Einstein condensation in dilute gases* (Cambridge university press, 2008).
- [8] M. Fattori, C. D’Errico, G. Roati, M. Zaccanti, M. Jonas-Lasinio, M. Modugno, M. Inguscio, and G. Modugno, Atom interferometry with a weakly interacting Bose-Einstein condensate, *Phys. Rev. Lett.* **100**, 080405 (2008).
- [9] M.-O. Mewes, M. R. Andrews, D. M. Kurn, D. S. Durfee, C. G. Townsend, and W. Ketterle, Output coupler for Bose-Einstein condensed atoms, *Phys. Rev. Lett.* **78**, 582 (1997).
- [10] C. Lee, J. Huang, H. Deng, H. Dai, and J. Xu, Nonlinear quantum interferometry with Bose condensed atoms, *Front. Phys.* **7**, 109 (2012).
- [11] O. Morsch, M. Cristiani, J. H. Müller, D. Ciampini, and E. Arimondo, Free expansion of a Bose-Einstein condensate in a one-dimensional optical lattice, *Phys. Rev. A* **66**, 021601(R) (2002).
- [12] O. Morsch and E. Arimondo, Ultracold atoms and Bose-Einstein condensates in optical lattices, in *Dynamics and Thermodynamics of Systems with Long-Range Interactions*, edited by T. Dauxois, S. Ruffo, E. Arimondo, and M. Wilkens (Springer Berlin Heidelberg, Berlin, Heidelberg, 2002) pp. 312–331.
- [13] W. Bao, D. Jaksch, and P. A. Markowich, Numerical solution of the Gross-Pitaevskii equation for Bose-Einstein condensation, *J. Comput. Phys.* **187**, 318 (2003).
- [14] X. Antoine, W. Bao, and C. Besse, Computational methods for the dynamics of the nonlinear Schrödinger/Gross-Pitaevskii equations, *Comp. Phys. Comm.* **184**, 2621 (2013).
- [15] M. M. Cerimele, M. L. Chiofalo, F. Pistella, S. Succi, and M. P. Tosi, Numerical solution of the Gross-Pitaevskii equation using an explicit finite-difference scheme: An application to trapped Bose-Einstein condensates, *Phys. Rev. E* **62**, 1382 (2000).
- [16] J. Polo and V. Ahufinger, Soliton-based matter-wave interferometer, *Phys. Rev. A* **88**, 053628 (2013).
- [17] S.-T. Ji, Y.-S. Wang, Y.-E. Luo, and X.-S. Liu, Generating periodic interference in Bose-Einstein condensates, *Chin. Phys. B* **25**, 090303 (2016).
- [18] V. Ahufinger, A. Sanpera, P. Pedri, L. Santos, and M. Lewenstein, Creation and mobility of discrete solitons in Bose-Einstein condensates, *Phys. Rev. A* **69**, 053604 (2004).
- [19] C. Ottaviani, V. Ahufinger, R. Corbalán, and J. Mompart, Adiabatic splitting, transport, and self-trapping of a Bose-Einstein condensate in a double-well potential, *Phys. Rev. A* **81**, 043621 (2010).
- [20] N. H. Berry and J. N. Kutz, Dynamics of Bose-Einstein condensates under the influence of periodic and harmonic potentials, *Phys. Rev. E* **75**, 036214 (2007).
- [21] Z. Yan and D. Jiang, Matter-wave solutions in Bose-Einstein condensates with harmonic and Gaussian potentials, *Phys. Rev. E* **85**, 056608 (2012).
- [22] K. Mallory and R. A. Van Gorder, Stationary solutions for the 1+1 nonlinear schrödinger equation modeling attractive Bose-Einstein condensates in small potentials, *Phys. Rev. E* **89**, 013204 (2014).
- [23] A. S. Sanz and S. Miret-Artés, *A Trajectory Description of Quantum Processes. I. Fundamentals*, Lecture Notes



- in Physics, Vol. 850 (Springer, Berlin, 2012).
- [24] A. S. Sanz, Bohm's approach to quantum mechanics: Alternative theory or practical picture?, *Front. Phys.* **14**, 11301 (2019).
- [25] A. Benseny, J. Bagudà, X. Oriols, G. Birkl, and J. Mompart, *Applied Bohmian Mechanics: From Nanoscale Systems to Cosmology*, edited by X. Oriols and J. Mompart (Pan Stanford Publishing, Singapore, 2012) Chap. Atomtronics: Coherent control of atomic flow via adiabatic passage, pp. 189–233.
- [26] S. L. Cornish, N. R. Claussen, J. L. Roberts, E. A. Cornell, and C. E. Wieman, Stable  $^{85}\text{Rb}$  Bose-Einstein condensates with widely tunable interactions, *Phys. Rev. Lett.* **85**, 1795 (2000).
- [27] C. C. Bradley, C. A. Sackett, J. J. Tollett, and R. G. Hulet, Evidence of Bose-Einstein condensation in an atomic gas with attractive interactions, *Phys. Rev. Lett.* **75**, 1687 (1995).
- [28] M. H. Anderson, J. R. Ensher, M. R. Matthews, C. E. Wieman, and E. A. Cornell, Observation of Bose-Einstein condensation in a dilute atomic vapor, *Science* **269**, 198 (1995).
- [29] K. B. Davis, M. O. Mewes, M. R. Andrews, N. J. van Druten, D. S. Durfee, D. M. Kurn, and W. Ketterle, Bose-Einstein condensation in a gas of sodium atoms, *Phys. Rev. Lett.* **75**, 3969 (1995).
- [30] S. Burger, K. Bongs, S. Dettmer, W. Ertmer, K. Sengstock, A. Sanpera, G. V. Shlyapnikov, and M. Lewenstein, Dark solitons in Bose-Einstein condensates, *Phys. Rev. Lett.* **83**, 5198 (1999).
- [31] T. F. Scott, R. J. Ballagh, and K. Burnett, Formation of fundamental structures in Bose-Einstein condensates, *J. Phys. B: At. Mol. Opt. Phys.* **31**, L329 (1998).
- [32] L. Dobrek, M. Gajda, M. Lewenstein, K. Sengstock, G. Birkl, and W. Ertmer, Optical generation of vortices in trapped Bose-Einstein condensates, *Phys. Rev. A* **60**, R3381 (1999).
- [33] P. G. Kevrekidis, D. J. Frantzeskakis, and R. Carretero-González, eds., *Emergent Nonlinear Phenomena in Bose-Einstein Condensates: Theory and Experiment* (Springer Berlin Heidelberg, Berlin, Heidelberg, 2008).
- [34] D. J. Frantzeskakis, Dark solitons in atomic Bose-Einstein condensates: from theory to experiments, *J. Phys. A: Math. Theor.* **43**, 213001 (2010).
- [35] T. Tsuzuki, Nonlinear waves in the pitaevskii-gross equation, *J. Low Temp. Phys.* **4**, 441 (1971).
- [36] N. G. Parker, N. P. Proukakis, M. Leadbeater, and C. S. Adams, Soliton-sound interactions in quasi-one-dimensional Bose-Einstein condensates, *Phys. Rev. Lett.* **90**, 220401 (2003).
- [37] J. P. Ronzheimer, *Interactions of Dark Solitons in Cigar Shaped Bose-Einstein Condensates*, Ph.D. thesis, Kirchhoff-Institut für Physik, University of Heidelberg, Germany (2008).
- [38] N. G. Parker, N. P. Proukakis, and C. S. Adams, Dark soliton decay due to trap anharmonicity in atomic Bose-Einstein condensates, *Phys. Rev. A* **81**, 033606 (2010).
- [39] E. Madelung, Quantentheorie in hydrodynamischer form, *Z. Phys.* **40**, 322 (1926).
- [40] D. Bohm, A suggested interpretation of the quantum theory in terms of “hidden” variables. I, *Phys. Rev.* **85**, 166 (1952).
- [41] D. Bohm, A suggested interpretation of the quantum theory in terms of “hidden” variables. II, *Phys. Rev.* **85**, 180 (1952).
- [42] L. I. Schiff, *Quantum Mechanics*, 3rd ed. (McGraw-Hill, Singapore, 1968).
- [43] P. R. Holland, *The Quantum Theory of Motion* (Cambridge University Press, Cambridge, 1993).
- [44] L. D. Landau, The theory of superfluidity of helium II, *J. Phys. (USSR)* **5**, 71 (1941).
- [45] L. Landau, Theory of the superfluidity of helium II, *Phys. Rev.* **60**, 356 (1941).
- [46] M. Lewenstein, A. Sanpera, V. Ahufinger, B. Damski, A. Sen(De), and U. Sen, Ultracold atomic gases in optical lattices: mimicking condensed matter physics and beyond, *Adv. Phys.* **56**, 243 (2007), <https://doi.org/10.1080/00018730701223200>.
- [47] P. J. Y. Louis, E. A. Ostrovskaya, and Y. S. Kivshar, Matter-wave dark solitons in optical lattices, *J. Opt. B: Quantum Semiclass. Opt.* **6**, S309 (2004).
- [48] R. Grimm, M. Weidemüller, and Y. B. Ovchinnikov, Optical dipole traps for neutral atoms (Academic Press, 2000) pp. 95–170.
- [49] I. Bloch, J. Dalibard, and W. Zwerger, Many-body physics with ultracold gases, *Rev. Mod. Phys.* **80**, 885 (2008).
- [50] A. Weller, *Dynamics and Interaction of Dark Solitons in Bose-Einstein Condensates*, Ph.D. thesis, University of Heidelberg, Germany (2009).
- [51] A. S. Sanz and S. Miret-Artés, A trajectory-based understanding of quantum interference, *J. Phys. A: Math. Theor.* **41**, 435303 (2008).
- [52] A. S. Sanz and S. Miret-Artés, *A Trajectory Description of Quantum Processes. II. Applications*, Lecture Notes in Physics, Vol. 831 (Springer, Berlin, 2014).
- [53] M. D. Feit and J. J. A. Fleck, Light propagation in graded-index optical fibers, *Appl. Opt.* **17**, 3990 (1978).
- [54] M. D. Feit and J. J. A. Fleck, Computation of mode properties in optical fiber waveguides by a propagating beam method, *Appl. Opt.* **19**, 1154 (1980).
- [55] M. D. Feit, J. J. A. Fleck, and A. Steiger, Solution of the Schrödinger equation by a spectral method, *J. Comput. Phys.* **47**, 412 (1982).
- [56] W. H. Press, s. A. Teukolsky, W. T. Vetterling, and B. P. Flannery, *Numerical Recipes in Fortran 90: The Art of Parallel Scientific Computing*, 2nd ed., Vol. 2nd (Cambridge University Press, Cambridge, 1996).
- [57] A. Tonomura, N. Osakabe, T. Matsuda, T. Kawasaki, J. Endo, S. Yano, and H. Yamada, Evidence for Aharonov-Bohm effect with magnetic field completely shielded from electron wave, *Phys. Rev. Lett.* **56**, 792 (1986).
- [58] C. Philippidis, D. Bohm, and R. D. Kaye, The Aharonov-Bohm effect and the quantum potential, *Nuovo Cim. B* **71**, 57 (1982).
- [59] A. S. Sanz and S. Miret-Artés, Aspects of nonlocality from a quantum trajectory perspective: A WKB approach to Bohmian mechanics, *Chem. Phys. Lett.* **445**, 350 (2007).

## SUPPLEMENTAL MATERIAL

Figures from the main text without the sets of Bohmian trajectories in order to better appreciate the corresponding density plots.

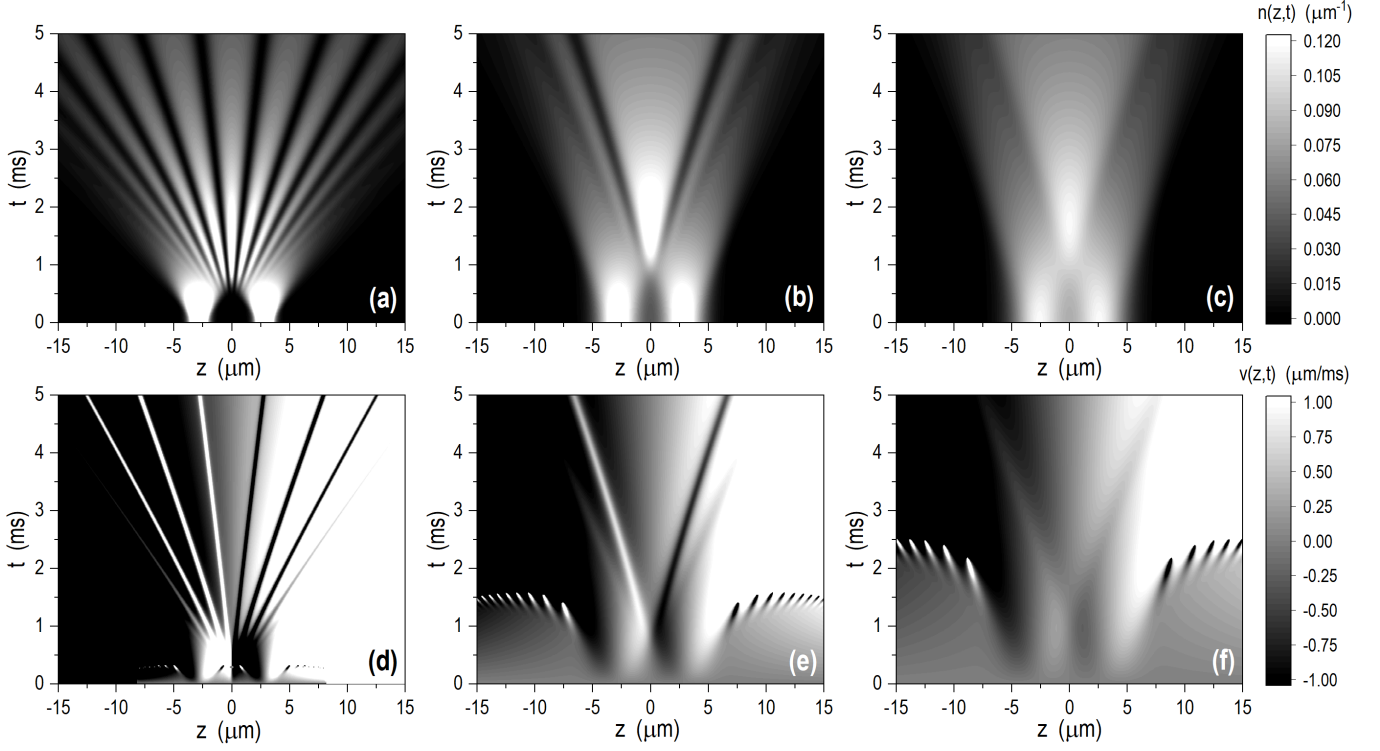


FIG. S3. Time-evolution of the BEC density distribution (top row) and its associated velocity field (lower row) for the three cases displayed in Fig. 2: (a/d)  $r = 1$ , (b/e)  $r = 2.5$ , and (c/f)  $r = 3.2$ . The color code to the right denotes the scale considered, from black for the lowest values of the quantities displayed to white for the highest values considered. For a better visualization and comparison, the density distributions have been truncated to  $0.12 \mu\text{m}^{-3}$ , while the velocity field ranges within  $\pm 1 \mu\text{m}/\text{ms}$ .

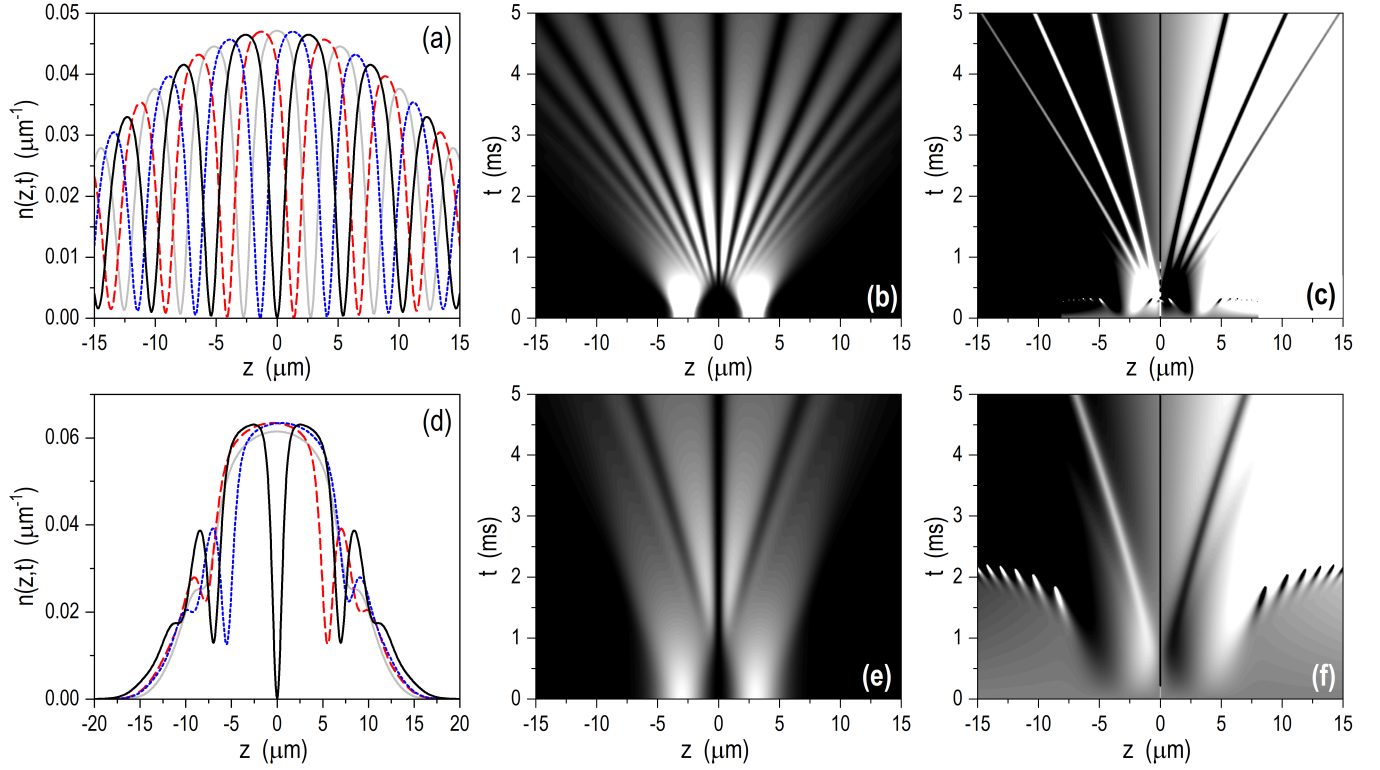


FIG. S4. Effect of the phase difference  $\phi$  on the dynamics exhibited by a coherent superposition of two condensates with identical Gaussian distributions, with peak-to-peak distance  $\ell = 5.7 \mu\text{m}$  and width  $\sigma_0 = r\sigma_{\text{eff}} \approx 0.49r \mu\text{m}$ . In the upper row, results for  $r = 1$ : (a) density profiles at  $t = 5$  ms for  $\phi = 0$  (solid gray line),  $\pi/2$  (dashed red line),  $\pi$  (solid black line), and  $-\pi/2$  (dotted blue line); (b) and (c) density plots showing the time evolution of the density distribution and the velocity field, respectively. In the lower row, the same for  $r = 3.2$ . The color code for panels (b), (c), (d), and (f) is the same as in Fig. S3.

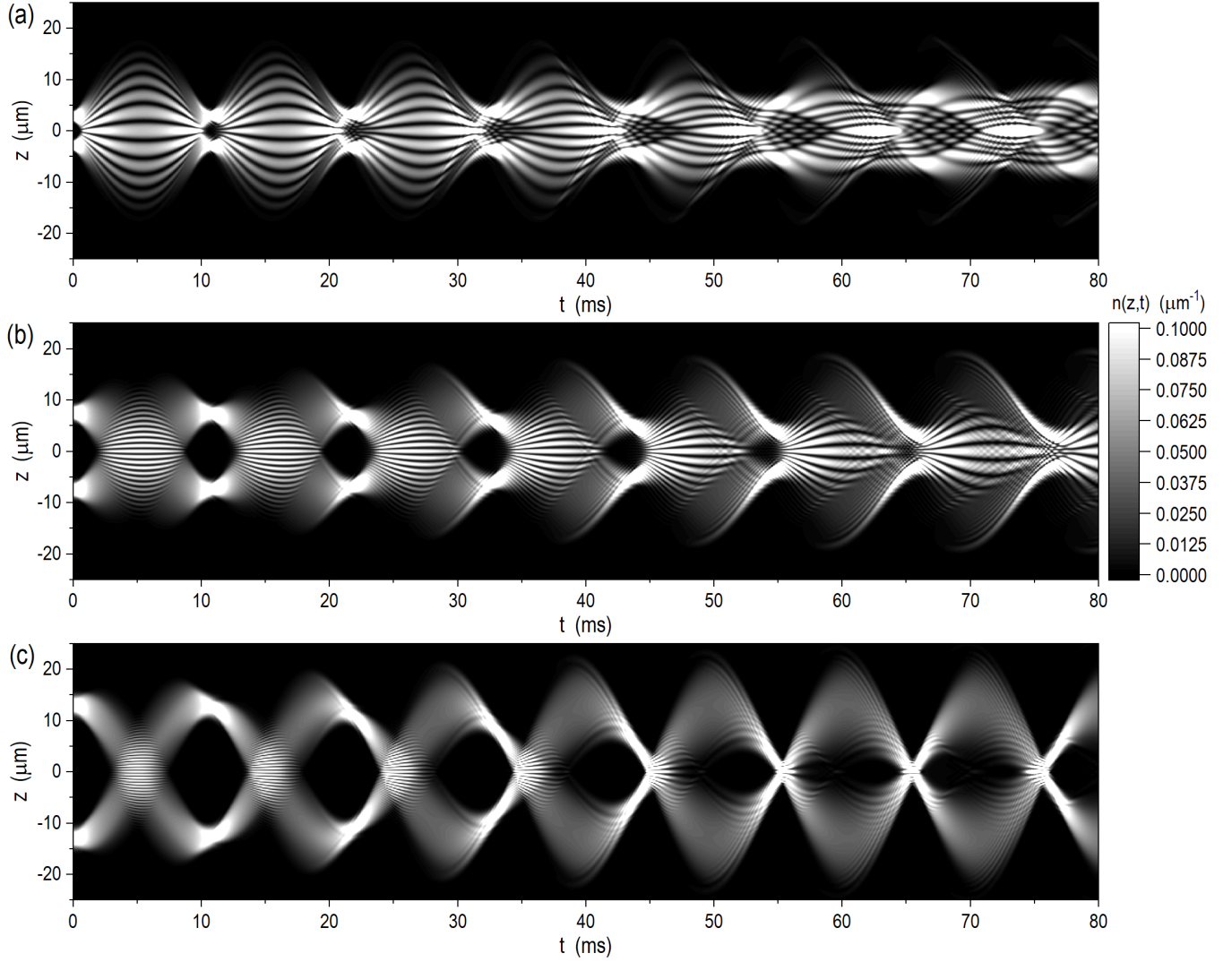


FIG. S5. Contour plots showing the time evolution of the density distribution associated with three initial superpositions with peak-to-peak distances: (a)  $\ell = 5.7 \mu\text{m}$ , (b)  $\ell = 15 \mu\text{m}$ , and (c)  $\ell = 26 \mu\text{m}$ . The color code is defined on the right; the distributions have been truncated to  $n_{\text{max}} = 0.1 \mu\text{m}^{-1}$  in all cases for a better visualization. In all cases the frequency of the harmonic trap is  $f_z = 50 \text{ Hz}$ .

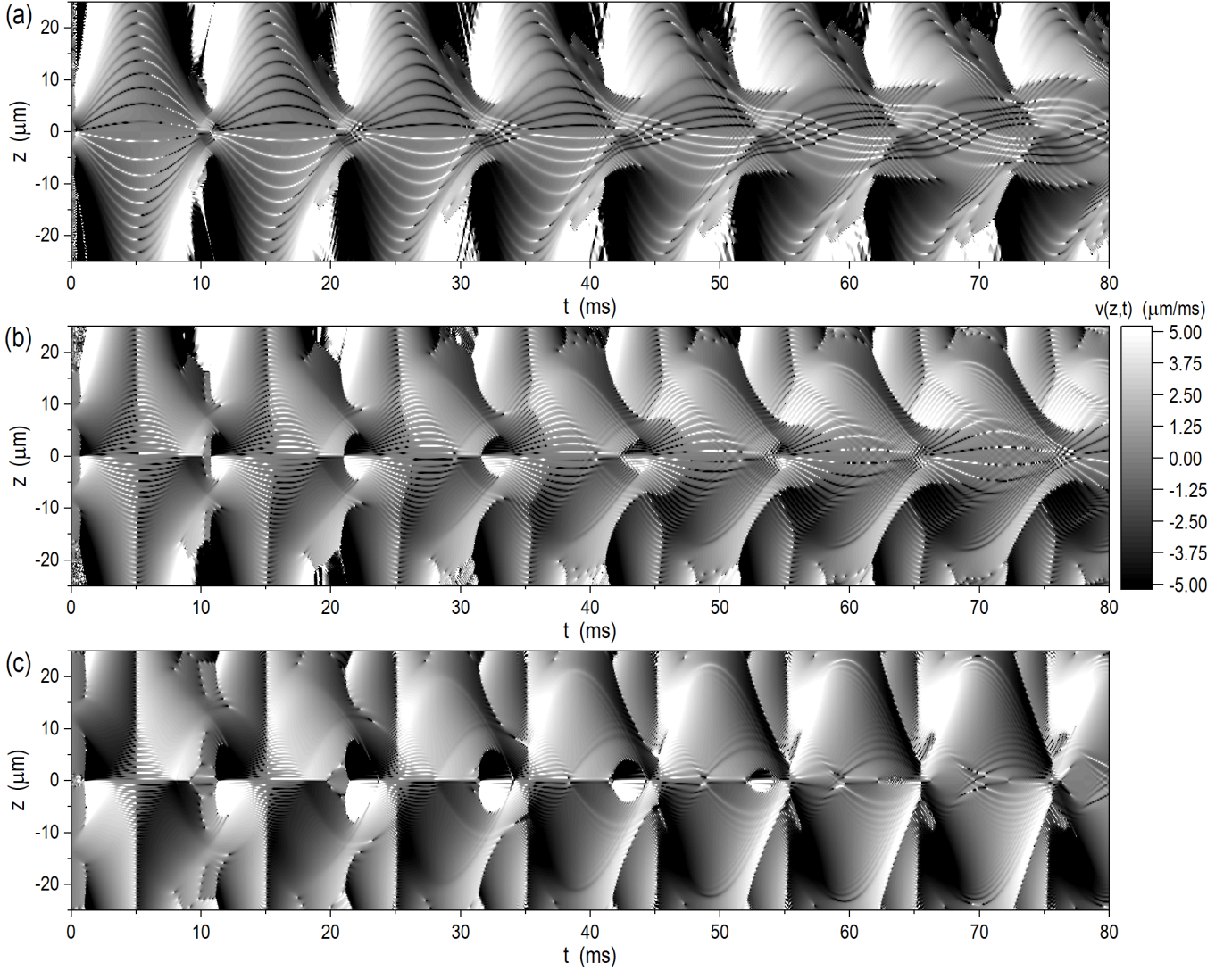


FIG. S6. Contour plots showing the time evolution of the velocity field associated with the three initial superpositions considered in Fig. 5, with peak-to-peak distances: (a)  $\ell = 5.7 \mu\text{m}$ , (b)  $\ell = 15 \mu\text{m}$ , and (c)  $\ell = 26 \mu\text{m}$ . The color code is defined on the right; velocity values have been constrained to the range  $\pm 5 \mu\text{m/ms}$  in all cases for a better visualization. In all cases the frequency of the harmonic trap is  $f_z = 50 \text{ Hz}$ .